Nonlinear Control for Proximity Operations Based on Differential Algebra

G. Di Mauro*
Dinamica Srl, 20156 Milan, Italy
M. Schlotterer† and S. Theil‡
DLR, German Aerospace Center, 28359 Bremen, Germany
and
M. Lavagna§
Politecnico di Milano, 20156 Milan, Italy

Nomenclature

$\boldsymbol{f}^{H}_{\text{control}}$	=	control acceleration vector expressed in Hill reference frame, m/s^2
$\boldsymbol{f}^{\text{HT}}_{\text{Thrust}}$	=	acceleration vector provided by testbed vehicle thrusters expressed in table inertial reference frame HT, m/s^2
I_C,I_T	=	inertia matrix of chaser, target satellite, $\text{kg} \cdot \text{m}^4$
I_V	=	inertia matrix of testbed vehicle, $\text{kg} \cdot \text{m}^4$
i	=	orbit inclination, rad
$\boldsymbol{q}_{A_1,A_2}$	=	quaternion vector representing relative attitude between $\boldsymbol{A}_1$ and A_2 reference frames, dim
$\boldsymbol{r}^{A_2}_{A_1}$	=	position vector of A_1 expressed in A_2 reference frame, m
$\boldsymbol{r}^{A_3}_{A_1,A_2}$	=	relative position vector between A_1 and A_2 expressed in A_3 reference frame, m
$\boldsymbol{T}^{V}_{\text{Thrust}}$	=	torque vector provided by testbed vehicle thrusters expressed in vehicle body-fixed reference frame V, Nm
θ	=	true anomaly, rad
$\boldsymbol{\Omega}$	=	right ascension of ascending node, rad
$\boldsymbol{\omega}^{A_3}_{A_1,A_2}$	=	angular velocity of A_1 with respect to A_2 expressed in A_3 reference frame, rad/s

I. Introduction

THE successful proximity operations during a docking maneuver involving two space vehicles has provoked great interest in last decade due to the continuous increase of space orbit activity. In fact, the rendezvous and docking (R&D) operation is a key element in missions that provide in-orbit assembling of large units, serving/refueling of orbital platforms and stations, malfunctioning satellite capturing, or installing improved technology.

The first rendezvous and docking between two spacecraft took place on 16 March 1966, when Neil Armstrong and Dave Scott manually performed a rendezvous in a Gemini vehicle and then docked with an unmanned Agena target vehicle. The first automatic R&D took place on 30 October 1967, when the Soviet vehicles Cosmos 186 and 188 docked, [1]. Thereafter, R&D operations have regularly been performed by the Russian, U.S. and European space programs. Among the most recent missions, the automated transfer vehicle program is worth being mentioned; it was developed by the ESA and designed to perform automated phasing, approach, rendezvous, and docking to the International Space Station, followed by departure and deorbit maneuvers, [2].

The main challenge related to the R&D maneuvering problem relies on the development of robust and reliable guidance, navigation, and control systems. Particularly, the proximity to the target spacecraft makes all operations safety critical, requiring particular safety features for trajectory design and a high-accuracy level for the control and navigation systems.

Because the R&D maneuvering control problem involves nonlinear kinematics and dynamics, in recent years, many nonlinear control methodologies have been investigated to address the relative motion control; some of these nonlinear techniques are inspired by the linear control theory, such as feedback linearization or gain scheduling, whereas others are inspired by stability Lyapunov theory of nonlinear systems, such as sliding mode control and adaptive control: In [3], Subbarao and Welsh have proposed an adaptive feedback linearization approach for attitude synchronization and relative position tracking; in [4], Terui has developed a sliding mode controller to regulate position and attitude for flight in proximity of a tumbling space object; Singla et al. developed an output feedback structured model reference adaptive control law for the spacecraft R&D problem and focused on analyzing the effect of bounded output errors on controller performance [5].

One of the most attractive methodologies for designing nonlinear controllers is the state-dependent Riccati equation (SDRE) approach, originally proposed by Pearson and then described in detail by Cloutier [6], Hammett [7], Beeler [8], and Cimen [9]. This method

Received 19 June 2014; revision received 20 January 2015; accepted for publication 29 January 2015; published online 9 April 2015.

*Senior Engineer, Via Morghen 13.
†Head of Guidance, Navigation, and Control (GNC) Department, Institute of Space Systems, Robert-Hooke-Strasse 7.
‡Researcher, Institute of Space Systems, Robert-Hooke-Strasse 7.
§Associate Professor, Aerospace Engineering Department, Via La Masa 34.

involves manipulating governing dynamic equations into a pseudo-linear nonunique form [referred to as the state-dependent coefficient (SDC) parameterization or extended linearization], in which system matrices are given as a function of the current state, and minimizing a quadratic-like performance index. Then, a suboptimal control law is carried out by an online solution of the algebraic Riccati equation (ARE) by means of a suited numerical algorithm. The SDRE approach is an effective option to issues involved with solving nonlinear Hamilton–Jacobi–Bellman partial differential equations associated with optimal nonlinear control problems; moreover, thanks to its formulation, it offers the same design flexibility of its linear counterpart, which is the linear quadratic regulator (LQR), allowing the designer to regulate the control signal magnitude by adjusting the entries in the penalty state-dependent matrices. On the other hand, it is sensitive to computational cost due to the online solution of an ARE, as illustrated in [10], where the SDRE method has been exploited to solve both formation-flying keeping and docking maneuvering problems. This aspect represents the main drawback of the SDRE technique, which might demand significantly more computational resources than conventional control algorithms, especially for high-order systems control. For this reason, the hardware implementation of the SDRE approach was scarce and restricted to low-order systems: Erdem and Alleyne exploited the SDRE technique to control a two-link underactuated, highly nonlinear nonminimum-phase robot dynamics [11]; Dang and Lewis conducted a real-time SDRE experiment for the swing up and balance of a single inverted pendulum on a linear track [12]; additionally, Menon et al. investigated the challenges associated with real-time implementation of SDRE control laws using Schur and Kleinman algorithms on a five-state variables system [13].

In light of the preceding, our study focuses on the development of an alternative approach to nonlinear optimal feedback control, aimed at reducing the computational cost of the SDRE method. The proposed approach exploits the differential algebra (DA) framework, which allows computing the Taylor expansion of a generic function f of $\boldsymbol{x}$ up to an arbitrary order v with a fixed amount of effort in a computer environment. Thus, the proposed DA-based algorithm enables one to obtain a high-order Taylor expansion of the SDRE solution of the relative motion problem around a reference trajectory. The main advantage of this new formulation is to reduce the computation of SDRE solution in a relatively large neighborhood of the reference trajectory to a mere evaluation of polynomials, avoiding the online solution of ARE and reducing the computational cost. Another important contribution of this research was the validation of the computational cost benefit of the proposed DA-based algorithm when it runs on a real hardware designed to emulate the proximity operations on ground.

The paper is organized as follows. In Sec. II, the SDRE controller for nonlinear optimal regulation is presented, reviewing some key aspects on stability and optimality; in the same section, the iterative Newton method for the SDRE solution is briefly reviewed. In Sec. III, a brief introduction to differential algebra is given and the DA-based algorithm is presented in detail. In Sec. IV, the relative orbital dynamics is discussed, wherein the relevant coordinate frames, governing equations of motion, and standing assumptions are detailed. In Sec. V, the guidance law used for the R&D maneuvers is described. Sections VI and VII present the platform developed by DLR, German Aerospace Center (DLR) Institute of Space Systems and exploited to carry out the experimental campaigns, and Sec. VIII illustrates the simulated scenario. Finally, the most relevant experimental results are gathered in Sec. IX.

II. State-Dependent Riccati Equation Technique

The SDRE strategy provides an effective and systematic algorithm to synthesize nonlinear feedback control by allowing nonlinearities in the system state. It is simply an extension of the constant-valued ARE used to find the optimal feedback control in the LQR problem. Let us consider the class of nonlinear in the state, affine in the input continuous-time systems described by the following:

$$\begin{aligned}\dot{\boldsymbol{x}}(t) &= \boldsymbol{f}(\boldsymbol{x}(t)) + \boldsymbol{g}(\boldsymbol{x}(t))\boldsymbol{U}(t)\\ \boldsymbol{y}(t) &= \boldsymbol{h}(\boldsymbol{x}(t))\\ \boldsymbol{x}(0) &= \boldsymbol{x}_0\end{aligned} \tag{1}$$

with the state vector $\boldsymbol{x} \in \boldsymbol{\Omega} \subseteq \mathfrak{R}^n$ and control $\boldsymbol{U} \in \mathfrak{R}^m$, such that $\boldsymbol{f}$: $\mathfrak{R}^n \to \mathfrak{R}^n$, $\boldsymbol{g}$: $\mathfrak{R}^n \to \mathfrak{R}^{n\times m}$, and $\boldsymbol{h}$: $\mathfrak{R}^s \to \mathfrak{R}^s$. The SDRE method approaches the problem by mimicking the LQR formulation for linear systems. Accordingly, the system of Eq. (1) can be written in a like-linear form as follows:

$$\begin{aligned}\dot{\boldsymbol{x}}(t) &= A(\boldsymbol{x})\boldsymbol{x} + B(\boldsymbol{x})\boldsymbol{U}\\ \boldsymbol{y}(t) &= H(\boldsymbol{x})\boldsymbol{x}\\ \boldsymbol{x}(0) &= \boldsymbol{x}_0\end{aligned} \tag{2}$$

where $\boldsymbol{f}(\boldsymbol{x}) = A(\boldsymbol{x})\boldsymbol{x}$, $\boldsymbol{g}(\boldsymbol{x}) = B(\boldsymbol{x})$, and $\boldsymbol{h}(\boldsymbol{x}) = H(\boldsymbol{x})\boldsymbol{x}$ with $A(\boldsymbol{x})$: $\boldsymbol{\Omega} \to \mathfrak{R}^{n\times n}$. The state-dependent dynamic matrix $A(\boldsymbol{x})$ is obtained by mathematical factorization and it is nonunique when $n > 1$. It is worth noting that the former parameterization, known as SDC parameterization or extended linearization, is possible if and only if the following conditions are satisfied [14,15]: 1) $\boldsymbol{f}(\boldsymbol{0}) = \boldsymbol{0}$ and $\boldsymbol{g}(\boldsymbol{x}) \neq \boldsymbol{0} \forall\ \boldsymbol{x}$; 2) $\boldsymbol{f}(\boldsymbol{x}) \in C^1$.

The optimal control problem is to find a state feedback control $\boldsymbol{U}$ that minimizes the cost functional for all possible initial conditions $\boldsymbol{x}_0$,

$$J(\boldsymbol{x}_0, \boldsymbol{U}) = \frac{1}{2}\int_0^\infty (\boldsymbol{x}^T Q(\boldsymbol{x})\boldsymbol{x} + \boldsymbol{U}^T Z(\boldsymbol{x})\boldsymbol{U})\mathrm{d}t \tag{3}$$

where the state and input weighting matrices $Q(\boldsymbol{x}) = H^T(\boldsymbol{x})H(\boldsymbol{x})$: $\mathfrak{R}^n \to \mathfrak{R}^{n\times n}$ and $Z(\boldsymbol{x})$: $\mathfrak{R}^n \to \mathfrak{R}^{m\times m}$ are assumed state dependent and positive semidefinite (PSD) and positive definite (PD), respectively, for all $\boldsymbol{x}$ to ensure the local stability [6,9,16]. If the pairs $(A(\boldsymbol{x}), B(\boldsymbol{x}))$ and $(H(\boldsymbol{x}), A(\boldsymbol{x}))$ are, respectively, pointwise stabilizable and a detectable extended linearization of the nonlinear system in the linear sense for all $\boldsymbol{x} \in \boldsymbol{\Omega}$, and conditions 1 and 2 are satisfied, the approximated solution of minimizing of the infinite-time performance criterion J is given by the following expression:

$$\boldsymbol{U} = -K(\boldsymbol{x})\boldsymbol{x}; \qquad K(\boldsymbol{x}) = Z^{-1}(\boldsymbol{x})B^T(\boldsymbol{x})P(\boldsymbol{x}) \tag{4}$$

where $K(\boldsymbol{x}) \in C^0$ and $P(\boldsymbol{x}) \in \mathfrak{R}^{n\times n}$ is the unique, symmetric positive-definite solution of the continuous-time state-dependent Riccati equation:

$$P(\boldsymbol{x})A(\boldsymbol{x}) + A^T(\boldsymbol{x})P(\boldsymbol{x}) - P(\boldsymbol{x})B(\boldsymbol{x})Z^{-1}(\boldsymbol{x})B(\boldsymbol{x})^T P(\boldsymbol{x}) + Q(\boldsymbol{x}) = 0 \tag{5}$$

In [9], the author states that a sufficient condition for stabilizability is to check that the $n \times nm$ state-dependent matrix

$$M_{\text{contr}} = [\,B(\boldsymbol{x}) \quad A(\boldsymbol{x})B(\boldsymbol{x}) \quad \cdots \quad A(\boldsymbol{x})^{n-1}B(\boldsymbol{x})\,] \tag{6}$$

has $\text{rank}(M_{\text{contr}}) = n\ \forall\ \boldsymbol{x} \in \boldsymbol{\Omega}$. Similarly, the sufficient test for the detectability is that the $n \times ns$ state-dependent matrix

$$M_{\text{obs}} = [\,H^T(\boldsymbol{x}) \quad A(\boldsymbol{x})^T H^T(\boldsymbol{x}) \quad \cdots \quad (A(\boldsymbol{x})^T)^{n-1}H^T(\boldsymbol{x})\,] \tag{7}$$

has $\text{rank}(M_{\text{obs}}) = n\ \forall\ \boldsymbol{x} \in \boldsymbol{\Omega}$.

Therefore, the SDRE solution for the infinite-time horizon nonlinear regulator problem (1–3) can be interpreted as a generalization of the infinite-time horizon time-invariant LQR problem, where all matrices are state dependent. The main advantages of the SDRE technique are simplicity and effectiveness, because no solution of the Hamilton–Jacobi–Bellman partial differential equation is required to solve the infinite-horizon nonlinear regulator problem, and design flexibility due to the

possibility of tuning the state and input weighting matrices Q and Z eventually depending on current state.

A thorough review of capabilities of the SDRE technique is provided by Cimen in [14]. Particularly, the author addresses the design flexibility of the SDRE method, showing a criterion to choose the state-dependent weighting matrices $Q(\boldsymbol{x})$ and $Z(\boldsymbol{x})$, and discusses the ability of SDRE controller to include the state/input constraints and to track a specific signal. In addition, in [9], Cimen investigates the stability and optimality properties associated with the SDRE controller, concluding that the SDRE method guarantees only local asymptotic stability and satisfies at least asymptotically the optimality conditions.

A. Numerical Algorithm for the Solution of Algebraic Riccati Equation

From a computation standpoint, the main efforts due to the SDRE algorithm implementation are related to the solution of high-dimensional ARE at each sample step. A closed-form solution of Eq. (5) is awkward except for a few simple dynamic systems, such that, in most problems, this equation will have to be numerically solved at each sample instant. Several numerical techniques exist for solving algebraic Riccati equations; particularly, these algorithms can be divided into two categories: 1) direct and 2) iterative methods. The former is based on manipulation of a Hamiltonian matrix (i.e., Schur decomposition), whereas the second determines iteratively the solution from an initial guess; generally, the direct methods are computationally faster than second, especially in poorly conditioned problems and in cases where a good initial guess is not available. On the other hand, the computation and storage requirements for them can be more than twice as much as that for an iterative method because the former operates on a $2n \times 2n$ Hamiltonian matrix for a Riccati equation of order n [13].

For the sake of completeness, a brief description of the Newton approach (iterative method) is presented in the following.

B. Iterative Method: Newton Method

Newton's method (NM) is a numerical tool for solving scalar nonlinear equations; given an equation $f(x) = 0$, where f is continuously differentiable in a neighborhood of a solution $\alpha \in$, Newton's method generates a sequence $\{x_k\}$ defined by $x_{k+1} = x_k - f(x_k)/f(x_k)^n$ which converges to α for a suitable initial guess x_0. The same approach can be used to solve the ARE (5) such that the following sequence is obtained [17–20]:

$$\begin{aligned} F(P_k) &= P_k A + A^T P_k - P_k B Z^{-1} B^T P_k + Q \\ P_{k+1} &= P_k - (F'_{P_k})^{-1}[F(P_k)] \end{aligned} \tag{8}$$

where F'_{P_k} indicates the Fréchet derivative of the rest function $F(P_k)$. In practical computation, the Newton increment $\Delta P_k = P_{k+1} - P_k$, is exploited, such that each Newton's method step yields

$$F'_{P_k}\Delta P_k = (A^T - P_k B)\Delta P_k + \Delta P_k (A - B P_k) = -[F(P_k)] \tag{9}$$

Equation (9) is a linear Lyapunov equation. In Algorithm 1, the main steps of NM are summarized. In [18], the authors demonstrate that the sequence $\{P_k\}$ converges quadratically to the stabilizing solution of ARE.

Algorithm 1 Newton method

1) Define the SDC for nonlinear system (1)
2) Set the initial guess P_0
3) Compute the rest function $F(P_k)$
4) Solve the Lyapunov equation $(A^T - P_k B)\Delta P_k + \Delta P_k (A - B P_k) = -[F(P_k)]$
5) Update the solution such that $P_{k+1} = P_k + \Delta P_k$
6) Iterate until the maximum number of iterations is reached or $\|\Delta P_k\|/\|P_k\| <$ toll

III. Differential Algebra Technique

The DA technique finds its origin in the attempt to solve analytical problems with an algebraic approach. One of the initiators of the field was Liouville in connection with the problem of integration of functions and differential equations in finite terms. It was then significantly enhanced by Ritt [21], who provided a complete algebraic theory of the solution of differential equations that are polynomials of the functions and their derivatives and that have meromorphic coefficients [22]. Recently, this approach was exploited to solve two-point value boundary problems, which is typically faced in space trajectory design [23]. DA serves the purpose of computing the derivatives of functions in a computer environment; more specifically, by substituting the classical implementation of real algebra with the implementation of a new algebra of Taylor polynomials, any function f of $\boldsymbol{x}$ can be expanded into its Taylor series up to an arbitrary order v. DA was implemented by Makino in the software COSY-Infinity.[¶] In what follows, the basis of differential algebra will be summarized; particularly, the minimal differential algebra for one-dimensional functions and their first-order expansion is explained in detail and some hints on its extension to functions of n variables and to vth order are given. Finally, we will focus on the use of the DA technique to determine an approximated solution of the SDRE problem.

A. Minimal Differential Algebra

To present the simplest nontrivial differential algebra, let us consider the set of all ordered pairs (p_0, p_1), with p_0 and p_1 real numbers. Define addition, scalar multiplication, and vector multiplication as follows:

$$\begin{aligned} (p_0, p_1) + (r_0, r_1) &= (p_0 + r_0, p_1 + r_1) \\ t \cdot (p_0, p_1) &= (t \cdot p_0, t \cdot p_1) \\ (p_0, p_1) \cdot (r_0, r_1) &= (p_0 \cdot r_0, p_0 \cdot r_1 + p_1 \cdot r_0) \end{aligned} \tag{10}$$

The ordered pairs with the preceding arithmetic are called ${}_1D_1$, and the three operations defined in Eq. (10) form an algebra. Furthermore, they do form an extension of real numbers; since $(r, 0) + (s, 0) = (r + s, 0)$ and $(r, 0) \cdot (s, 0) = (r \cdot s, 0)$, the pairs $(r, 0)$ behave like real numbers [22].

One important property of this algebra is that it has an order compatible with its algebraic operations. Particularly, given two elements (p_0, p_1) and (r_0, r_1) in ${}_1D_1$, it results

$$\begin{aligned} &(p_0, p_1) < (r_0, r_1) \quad \text{if } p_0 < r_0 \quad \text{or} \quad (p_0 = r_0 \text{ and } p_1 < r_1) \\ &(p_0, p_1) > (r_0, r_1) \quad \text{if } (r_0, r_1) < (p_0, p_1) \\ &(p_0, p_1) = (r_0, r_1) \quad \text{if } p_0 = r_0 \quad \text{and} \quad p_1 = r_1 \end{aligned} \tag{11}$$

As for any two elements (p_0, p_1) and $(r_0, r_1) \in {}_1D_1$, only one of the three relations (11) holds, ${}_1D_1$ is said totally ordered [22].

In ${}_1D_1$, the number $d = (0, 1)$ plays an important role; it has the interesting property of being positive but smaller than any positive real number, such that $(0, 0) < (0, 1) < (r, 0) = r$. For this reason d is called an infinitesimal or a differential, and, in fact, d is so small that it vanishes in ${}_1D_1$. Because for any $(p_0, p_1) \in {}_1D_1$,

$$(p_0, p_1) = (p_0, 0) + (0, p_1) = p_0 + d \cdot p_1 \tag{12}$$

the first component p_0 is called the real part and the second p the differential part. The aforementioned algebra becomes a differential algebra by introducing a map ∂: ${}_1D_1 \to {}_1D_1$ and proving that the map is a derivation. Define ∂: ${}_1D_1 \to {}_1D_1$ by

$$\partial(p_0, p_1) = (0, p_1) \tag{13}$$

[¶]Data available online at http://www.bt.pa.msu.edu/index_cosy.htm [retrieved 9 July 2014].

The map ∂ is a derivation because, for all $(p_0, p_1), (r_0, r_1) \in {}_1D_1$, it results

$$\begin{aligned}
&\partial\{(p_0, p_1) + (r_0, r_1)\} = \partial(p_0 + r_0, p_1 + r_1) = (0, p_1 + r_1) \\
&\quad = (0, p_1) + (0, r_1) = \partial(p_0, p_1) + \partial(r_0, r_1) \\
&\partial\{(p_0, p_1) \cdot (r_0, r_1)\} = \partial(p_0 \cdot r_0, p_0 \cdot r_1 + r_0 \cdot p_1) \\
&\quad = (0, p_0 \cdot r_1 + r_0 \cdot p_1) = (0, p_1) \cdot (r_0, r_1) + (0, r_1) \cdot (p_0, p_1) \\
&\quad = \partial\{(p_0, p_1)\} \cdot (r_0, r_1) + (p_0, p_1) \cdot \partial\{(r_0, r_1)\} \qquad (14)
\end{aligned}$$

Thus, $({}_1D_1, \partial)$ is a differential algebra. For the purpose of nonlinear controller design, the most important aspect of ${}_1D_1$ is that it can be used for the automated computation of derivatives. As an example, consider two functions f and g and arrange their values and their derivatives at the origin as two vectors in ${}_1D_1$, that is, $(f(0), f'(0))$ and $(g(0), g'(0))$. The product of two vectors $(f(0), f'(0))$ and $(g(0), g^n(0))$ yields

$$\begin{aligned}
&(f(0), f'(0)) \cdot (g(0), g'(0)) \\
&\quad = (f(0) \cdot g(0), f(0) \cdot g'(0) + f'(0) \cdot g(0)) \qquad (15)
\end{aligned}$$

Thus, the derivate of the product $f(0) \cdot g(0)$ appears in the second term of $(f(0), f'(0)) \cdot (g(0), g'(0)))$, whereas the first term gives the value of the product of the functions. Therefore, if two vectors contain the values and the derivatives of two functions, their product contains the values and the derivatives of the product function. Defining the operation $[\cdot]$ from the space of differential functions to ${}_1D_1$ as

$$[f] = (f(0), f'(0)) \qquad (16)$$

it holds that

$$[f + g] = [f] + [g] \quad [f \cdot g] = [f] \cdot [g] \quad [1/g] = \frac{1}{[g]} \qquad (17)$$

In light of the preceding, derivatives of many kinds of functions can be computed algebraically by applying arithmetic rules on ${}_1D_1$, beginning from the value and the derivative of the identity function $[x] = (x, 1) = x + d$. In fact, it is possible to prove that the following results [22]

$$[f(x)] = (f(x), f'(x)) = f((x + d)) = f([x]) \qquad (18)$$

It is worth noting that, for $r \in \mathfrak{R} \subset {}_1D_1$, $(f(r), f'(r)) = f(r + d) = f(r) + d \cdot f'(r))$ resembles $f(x + \Delta x) \approx f(x) + \Delta x \cdot f'(x)$, in which the approximation becomes more refined for smaller Δx.

B. Differential Algebra ${}_vD_n$

In the following subsection, we introduce the algebra to compute the derivatives of a function in n variables up to the order v. Let us consider the space $C^v(\mathfrak{R}^n)$, that is, the collection of v times continuously differentiable functions on $\mathfrak{R}^n$. On this space, we introduce an equivalence relation $=_v$, such that, given the functions f and $g \in C^v(\mathfrak{R}^n)$, $f =_v g$ if and only if $f(0) = g(0)$ and all the partial derivatives agree at zero up to the order v. The relation $=_v$ satisfies [22]

$$\begin{aligned}
&f =_v f \qquad \text{for all } f \in C^v(\mathfrak{R}^n) \\
&f =_v g \Rightarrow g =_v f \qquad \text{for all } f, g \in C^v(\mathfrak{R}^n) \\
&f =_v g \quad \text{and} \quad g =_v w \Rightarrow f =_v w \qquad \text{for all } f, g, w \in C^v(\mathfrak{R}^n)
\end{aligned} \qquad (19)$$

All the elements that are related to f can be grouped together in one set, the equivalence class $[f]$ of the function f. The resulting equivalence classes are referred to as DA vectors or DA numbers. Intuitively, each of these classes is specified by a particular collection of partial derivatives in all n variables up to order v. This class is called ${}_vD_n$, and it represents an algebra [22]. In addition, it is easy to show, and its proof is omitted here because it is beyond the purpose of this paper, that, defined the map $\partial_k \colon {}_vD_n \to {}_vD_n$ for $k \in 1 \ldots n$ as

$$\partial_k[f] = \left[x_k \frac{\partial f}{\partial x_k}\right] \quad \text{with } [f] \in {}_vD_n \qquad (20)$$

it is a derivation for all k, and hence $({}_vD_n, \partial_1, \ldots, \partial_k))$ is a differential algebra.

Observe that f lies in the same class as its Taylor polynomial T_f of order v around the origin; they have the same function values and derivatives up to order v. Therefore,

$$[f] = [T_f] \qquad (21)$$

where

$$\begin{aligned}
[T_f] &= \left[\sum_{j_1 + \ldots + j_n \le v} c_{j_1, \ldots, j_n} \cdot x_1^{j_1} \ldots x_n^{j_n}\right] \\
&= \sum_{j_1 + \ldots + j_n \le v} c_{j_1, \ldots, j_n} \cdot d_1^{j_1} \ldots d_n^{j_n} \qquad (22)
\end{aligned}$$

being $d_k = [x_k]$ and $c_{j_1, \ldots, j_n}$ the Taylor coefficients of the Taylor polynomial T_f defined as

$$c_{j_1, \ldots, j_n} = \frac{1}{j_1! \ldots j_n!} \cdot \frac{\partial^{j_1 + \ldots + j_n} f}{\partial x_1^{j_1} \ldots \partial x_n^{j_n}} \qquad (23)$$

Similarly to ${}_1D_1$, composition of functions and the elementary functions, as trigonometric or exponential functions, can be introduced in ${}_vD_n$; thus, the derivatives of any function f belonging to $C^v(\mathfrak{R}^n)$ can be computed up to order v with a fixed amount of effort by applying

$$[f(x_1 \ldots x_n)] = f[(x_1 \ldots x_n)] = f(x_1 + d_1, \ldots, x_n + d_n) \qquad (24)$$

For more details about the preceding presented differential algebra, we address the reader to [22].

C. Differential Algebra Approach: High-Order Technique for SDRE Solution

In our work, differential algebra is effectively used to get a high-order Taylor expansion of the SDRE solution. For this purpose, consider a power series expansion of $P(\boldsymbol{x})$ in Eq. (5) in terms of temporary variable ε, such that

$$P(\boldsymbol{x}) = \sum_{k=0}^{\infty} \varepsilon^k P_k(\boldsymbol{x}) \cong \sum_{k=0}^{l} \varepsilon^k P_k(\boldsymbol{x}) \qquad (25)$$

and split the dynamic matrices $A(\boldsymbol{x})$ and $B(\boldsymbol{x})$ obtained by the SDC parameterization into constant and state-dependent parts as

$$A(\boldsymbol{x}) = A_0 + \varepsilon \Delta A(\boldsymbol{x}); \qquad B(\boldsymbol{x}) = B_0 + \varepsilon \Delta B(\boldsymbol{x}) \qquad (26)$$

Substituting Eqs. (25) and (26) in Eq. (5) and separating out by powers of ε, the following series of equations result:

$$P_0 A_0 + A_0^T P_0 - P_0 B_0 Z^{-1} B_0^T P_0 + Q = 0 \qquad (27)$$

$$
\begin{aligned}
&P_k(\boldsymbol{x})\tilde{A} + \tilde{A}^T P_k(\boldsymbol{x}) = -P_{k-1}(\boldsymbol{x})\Delta A(\boldsymbol{x}) - \Delta A(\boldsymbol{x})^T P_{k-1}(\boldsymbol{x}) \\
&\quad + \sum_{j=1}^{k-1} P_j(\boldsymbol{x})(B_0 Z^{-1} B_0^T) P_{k-j}(\boldsymbol{x}) \\
&\quad = + \sum_{j=0}^{k-1} P_j(\boldsymbol{x})(B_0 Z^{-1} \Delta B(\boldsymbol{x})^T + \Delta B(\boldsymbol{x}) Z^{-1} B_0) P_{k-1-j}(\boldsymbol{x}) \\
&\quad = + \sum_{j=0}^{k-2} P_j(\boldsymbol{x})(\Delta B(\boldsymbol{x}) Z^{-1} \Delta B(\boldsymbol{x})^T) P_{k-2-j}(\boldsymbol{x}) \qquad k = 1, \ldots, 1
\end{aligned}
\tag{28}
$$

where

$$
\tilde{A} = (A_0 - B_0 Z^{-1} B_0^T P_0) \tag{29}
$$

and weighting matrices Z and Q are constant for simplicity.

Equation (27) is an algebraic Riccati equation where all matrices are constant, whereas Eqs. (28) are a series of linear Lyapunov equations that can be solved through linear algebra manipulation, as discussed in [24], or more efficiently, through the Bartels and Stewart algorithm [17,25].

Now, let us initialize the state vector $\boldsymbol{x}$ in Eqs. (25) and (26) as a vth order DA variable, that is,

$$
[\boldsymbol{x}] = \boldsymbol{x}^0 + \delta\boldsymbol{x} \tag{30}
$$

such that matrices P_k in Eqs. (28), ΔA and ΔB in Eq. (26) are function of $\delta\boldsymbol{x}$,

$$
\begin{aligned}
&P_k(\delta\boldsymbol{x})\tilde{A} + \tilde{A}^T P_k(\delta\boldsymbol{x}) = -P_{k-1}(\delta\boldsymbol{x})\Delta A(\delta\boldsymbol{x}) - \Delta A(\delta\boldsymbol{x})^T P_{k-1}(\delta\boldsymbol{x}) \\
&\quad + \sum_{j=1}^{k-1} P_j(\delta\boldsymbol{x})(B_0 Z^{-1} B_0^T) P_{k-j}(\delta\boldsymbol{x}) \\
&\quad = + \sum_{j=0}^{k-1} P_j(\delta\boldsymbol{x})(B_0 Z^{-1} \Delta B(\delta\boldsymbol{x})^T + \Delta B(\delta\boldsymbol{x}) Z^{-1} B_0) P_{k-1-j}(\delta\boldsymbol{x}) \\
&\quad = + \sum_{j=0}^{k-2} P_j(\delta\boldsymbol{x})(\Delta B(\delta\boldsymbol{x}) Z^{-1} \Delta B(\delta\boldsymbol{x})^T) P_{k-2-j}(\delta\boldsymbol{x}) \\
&\quad k = 1, \ldots, 1
\end{aligned}
\tag{31}
$$

Thus, the feedback control law results

$$
\begin{aligned}
&\boldsymbol{U}^v_{\mathrm{SDRE/DA}}(\delta\boldsymbol{x}) = -Z^{-1}(B_0 + \Delta B(\delta\boldsymbol{x}))^T \left(\sum_{k=0}^{l} P_k(\delta\boldsymbol{x}) \right) \delta\boldsymbol{x} \\
&\quad = \tilde{K}(\delta\boldsymbol{x})\delta\boldsymbol{x} \quad \text{with } \varepsilon \text{ set to 1} \\
&\tilde{K}(\delta\boldsymbol{x}) = \begin{bmatrix} T_{\tilde{K}_{11}}(\delta\boldsymbol{x}) & \ldots & T_{\tilde{K}_{1n}}(\delta\boldsymbol{x}) \\ \vdots & \ddots & \vdots \\ T_{\tilde{K}_{m1}}(\delta\boldsymbol{x}) & \ldots & T_{\tilde{K}_{mn}}(\delta\boldsymbol{x}) \end{bmatrix} \\
&T_{\tilde{K}_{pq}}(\delta\boldsymbol{x}) = \sum_{j_1 + \ldots + j_n \le v} c_{j_1, \ldots j_n} \cdot \delta\boldsymbol{x}_1^{j_1} \ldots \delta\boldsymbol{x}_n^{j_n} \\
&p = 1, \ldots, m; \qquad q = 1, \ldots, n \\
&c_{j_1, \ldots j_n} = \frac{1}{j_1! \ldots j_n!} \cdot \frac{\partial^{j_1 + \ldots + j_n}(\tilde{K}_{pq}(\boldsymbol{x}))}{\partial\boldsymbol{x}_1^{j_1} \ldots \partial\boldsymbol{x}_n^{j_n}}
\end{aligned}
\tag{32}
$$

where $T_{\tilde{K}_{pq}}(\delta\boldsymbol{x})$ denotes the Taylor polynomial of order v of $\tilde{K}_{pq}(\boldsymbol{x})$, whereas $c_{j_1, \ldots j_n}$ are the Taylor coefficients of $T_{\tilde{K}_{pq}}(\delta\boldsymbol{x})$. Note that $\boldsymbol{U}^v_{\mathrm{SDRE/DA}}(\delta\boldsymbol{x})$ represents the deviation of control law from its reference value, given by

Algorithm 2 DA algorithm

1) Define the SDC for nonlinear system (1), $A(\boldsymbol{x})$ and $B(\boldsymbol{x})$
2) Compute the matrices $\Delta A(\boldsymbol{x}) = A(\boldsymbol{x}) - A_0$, $\Delta B(\boldsymbol{x}) = B(\boldsymbol{x}) - B_0$
3) Define the control state vector $\boldsymbol{x}$ as a DA vector $[\boldsymbol{x}] = \boldsymbol{x}^0 + \delta\boldsymbol{x}$;
4) Compute $\Delta A(\delta\boldsymbol{x})$ and $\Delta B(\delta\boldsymbol{x})$, and solve Eqs. (31) and (32) using COSY-Infinity to obtain Taylor map of control law

$$
\boldsymbol{U}^0_{\mathrm{SDRE/DA}} = -Z^{-1}(B_0 + \Delta B(\boldsymbol{x} = \boldsymbol{x}^0))^T \left(\sum_{k=0}^{l} P_k(\boldsymbol{x} = \boldsymbol{x}^0) \right) \boldsymbol{x}^0 \tag{33}
$$

The Taylor polynomials of order $vT_{\tilde{K}_{pq}}(\delta\boldsymbol{x})$ are obtained solving linear Lyapunov equations (31) in the COSY-Infinity code. In Algorithm 2, the DA-based algorithm is summarized.

Note that the computation of Taylor expansion of the controller matrix is carried out offline (see point 4 in Algorithm 2) by the COSY-Infinity tool, whereas the polynomial evaluation is performed online. The advantage of the presented method is evident: The SDRE solution is reduced to a mere evaluation of a polynomial expression instead of an online implementation of the procedure for an ARE solution. This fact makes the DA-based algorithm appealing for the real-time implementation of the SDRE technique.

IV. Spacecraft Relative Motion Dynamics

In following section, we provide the relative dynamics of two spacecraft orbiting the Earth, referred to as the chaser and target, and discuss a specific approaching trajectory to perform the R&D maneuver. In what follows, we will refer to the orbital reference frame (ORF), body-fixed reference frame (BRF), and Earth-centered inertial reference frame (ECIRF) (see Fig. 1). The ORF, denoted as H and known also as the Hill reference frame, is centered in the target center of mass and has the versors $\hat{\boldsymbol{r}}$ and $\hat{\boldsymbol{h}}$ aligned with the radial direction and the angular momentum, respectively. The BRFs, denoted as C and T for chaser and target, respectively, have the three axes oriented as the inertial principal axes and they are located in the center of mass of each spacecraft; note that, without loss of generality, we assume that $\hat{\boldsymbol{j}}_C$ and $-\hat{\boldsymbol{j}}_T$ are designed to be the outward direction of the chaser and target docking port (see Fig. 1). The ECIRF, denoted as I, is centered in Earth and it has the $\hat{\boldsymbol{K}}$ vector aligned with the Earth rotation axis (toward the North Pole), $\hat{\boldsymbol{I}}$ directed toward the vernal equinox, and $\hat{\boldsymbol{J}}$ completes the right-handed orthogonal reference frame.

A. Relative Dynamics Equations

Defining the relative position vector (see Fig. 1) $\boldsymbol{\rho}^H = x\hat{\boldsymbol{r}} + y\hat{\boldsymbol{t}} + z\hat{\boldsymbol{h}}$ and relative velocity vector $\dot{\boldsymbol{\rho}}^H = \dot{x}\hat{\boldsymbol{r}} + \dot{y}\hat{\boldsymbol{t}} + \dot{z}\hat{\boldsymbol{h}}$, the relative translation dynamics is given by [26]

$$
\begin{aligned}
\ddot{\boldsymbol{\rho}}^H = &-2[\boldsymbol{\omega}^H_{H,I} \wedge]\dot{\boldsymbol{\rho}}^H - [\boldsymbol{\omega}^H_{H,I} \wedge][\boldsymbol{\omega}^H_{H,I} \wedge]\boldsymbol{\rho}^H - [\dot{\boldsymbol{\omega}}^H_{H,I} \wedge]\boldsymbol{\rho}^H \\
&+ \frac{\mu}{\|\boldsymbol{r}^H_T + \boldsymbol{\rho}^H\|^3}(\boldsymbol{r}^H_T + \boldsymbol{\rho}^H) + \frac{\mu}{\|\boldsymbol{r}^H_T\|^3}(\boldsymbol{r}^H_T) + \\
&+ \boldsymbol{f}^H_{C,\mathrm{ext}} - \boldsymbol{f}^H_{T,\mathrm{ext}}
\end{aligned}
\tag{34}
$$

where $[\cdot\wedge]$ denotes the cross-product matrix. The vectors $\boldsymbol{f}^H_{T,\mathrm{ext}}$ and $\boldsymbol{f}^H_{C,\mathrm{ext}}$ represent the total external accelerations experienced by the target and chaser satellites, respectively. It is worth noting that the presence of perturbing acceleration provokes the precession of the Hill reference frame. More specifically, the angular velocity of H with respect to I, $\boldsymbol{\omega}^H_{H,I}$ is given by the sum of the instantaneous rate of three Eulerian angles regarded as vectors along the $\hat{\boldsymbol{K}}$ versor, the ascending node axis versor $\hat{\boldsymbol{N}}$, and $\hat{\boldsymbol{h}}$ directions, such that [27,28]

$$
\boldsymbol{\omega}^H_{H,I} = \dot{\Omega}\,\hat{\boldsymbol{K}} + \dot{i}\,\hat{\boldsymbol{N}} + \dot{\theta}\,\hat{\boldsymbol{h}} \tag{35}
$$

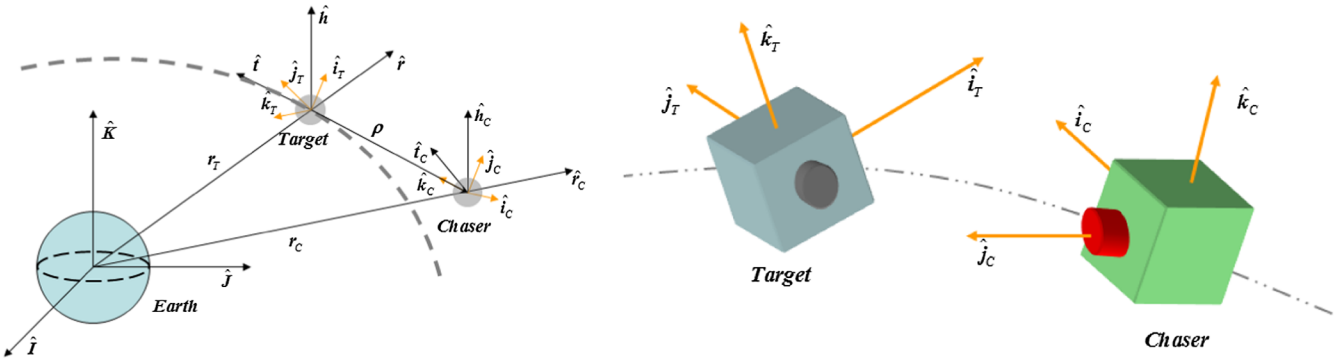

a) b)

Fig. 1 Reference frames: a) orbital $H = \{\hat{r} \quad \hat{t} \quad \hat{h}\}$; b) body $C = \{\hat{i}_C \quad \hat{j}_C \quad \hat{k}_C\}$; and $T = \{\hat{i}_T \quad \hat{j}_T \quad \hat{k}_T\}$.

By the inspection of orbital geometry, the unit vectors $\hat{N}$ and $\hat{K}$ can be written in the Hill system as

$$\begin{aligned}\hat{N} &= \cos(\theta)\hat{r} - \sin(\theta)\hat{t}\\ \hat{K} &= \sin(i)\sin(\theta)\hat{r} + \sin(i)\cos(\theta)\hat{t} + \cos(i)\hat{h}\end{aligned} \tag{36}$$

and thus,

$$\begin{aligned}\boldsymbol{\omega}_{H,I}^{H} &= [\dot{\Omega}\sin(i)\sin(\theta) + \dot{i}\cos(\theta)]\hat{r}\\ &+ [\dot{\Omega}\sin(i)\cos(\theta) - \dot{i}\sin(\theta)]\hat{t} + [\dot{\theta} + \dot{\Omega}\cos(i)]\hat{h}\\ &= \omega_x\hat{r} + \omega_y\hat{t} + \omega_z\hat{h}\end{aligned} \tag{37}$$

Finally, according to the Lagrange–Gauss equations, Eq. (37) yields

$$\boldsymbol{\omega}_{H,I}^{H} = \frac{r_T f_{\text{pert},h}}{h}\hat{r} + \frac{h}{r_T^2}\hat{h} = \omega_x\hat{r} + \omega_z\hat{h} \tag{38}$$

where $f_{\text{pert},h}$ indicates the component of perturbing acceleration orthogonal to the target orbital plane, and h is the modulus of the orbital angular momentum of the target spacecraft orbit. From Eq. (38), it results that the angular rate of the Hill reference frame has only components along $\hat{r}$ and $\hat{h}$, and it is always contained in the target orbital plane; this is consistent with the orbital problem: In fact, a rotation about $\hat{t}$ would move the orbit plane so as not to intersect the center of attraction, violating the Keplerian nature of the spacecraft orbital motion. Consistently, the angular acceleration of H is given by [29]

$$\begin{aligned}\dot{\boldsymbol{\omega}}_{H,I}^{H} &= \left(\frac{\dot{r}_T f_{\text{pert},h}}{h} + \frac{r_T \dot{f}_{\text{pert},h}}{h} - \frac{r_T^2 f_{\text{pert},h} f_{\text{pert},t}}{h^2}\right)\hat{r}\\ &+ \left(\frac{f_{\text{pert},t}}{r_T} - 2\frac{h\dot{r}_T}{r_T^3}\right)\hat{t}\end{aligned} \tag{39}$$

where $f_{\text{pert},t}$ indicates the component of perturbing acceleration aligned with $\hat{t}$ direction. Whenever the disturbance accelerations due to the space environment are ignored, Eq. (34) can be simplified; thus, the angular velocity and acceleration vectors of H relative to I, $\boldsymbol{\omega}_{H,I}^{H}$ and $\dot{\boldsymbol{\omega}}_{H,I}^{H}$ are given by

$$\boldsymbol{\omega}_{H,I}^{H} = \frac{h}{r_T^2}\hat{h} \qquad \dot{\boldsymbol{\omega}}_{H,I}^{H} = -2\frac{h\dot{r}_T}{r_T^3}\hat{h} \tag{40}$$

Therefore, the vector expression (34) can be written as three scalar nonlinear equations:

$$\begin{aligned}\ddot{x} &= y\left(-2\frac{h\dot{r}_T}{r_T^3}\right) + 2\dot{y}\left(\frac{h}{r_T^2}\right) + \boldsymbol{x}\left(\frac{h}{r_T^2}\right)^2\\ &- \frac{\mu(r_T + x)}{\sqrt{[(r_T + x)^2 + y^2 + z^2]^3}} + \frac{\mu}{r_T^2} + f_{x,\text{control}}^{H}\\ \ddot{y} &= x\left(2\frac{h\dot{r}_T}{r_T^3}\right) - 2\dot{x}\left(\frac{h}{r_T^2}\right) + y\left(\frac{h}{r_T^2}\right)^2\\ &- \frac{\mu y}{\sqrt{[(r_T + x)^2 + y^2 + z^2]^3}} + f_{y,\text{control}}^{H}\\ \ddot{z} &= -\frac{\mu z}{\sqrt{[(r_T + \boldsymbol{x})^2 + y^2 + z^2]^3}} + f_{z,\text{control}}^{H}\\ \boldsymbol{f}_{\text{control}}^{H} &= [f_{x,\text{control}}^{H} \quad f_{y,\text{control}}^{H} \quad f_{z,\text{control}}^{H}]^T\end{aligned} \tag{41}$$

being $\boldsymbol{f}_{C,\text{ext}}^{H} = \boldsymbol{f}_{\text{control}}^{H}$.

In addition, according with the well-known Euler's law, the rotational dynamics of the target and chaser spacecraft can be written as follows [30]

$$\dot{\boldsymbol{\omega}}_{T,I}^{T} = I_T^{-1}(-[\boldsymbol{\omega}_{T,I}^{T}\wedge]I_T\boldsymbol{\omega}_{T,I}^{T} + \boldsymbol{T}_{\text{ext}}^{T}) \tag{42}$$

$$\dot{\boldsymbol{\omega}}_{C,I}^{C} = I_C^{-1}(-[\boldsymbol{\omega}_{C,I}^{C}\wedge]I_C\boldsymbol{\omega}_{C,I}^{C} + \boldsymbol{T}_{\text{ext}}^{C}) \tag{43}$$

where the inertia matrices I_T and I_C are assumed to be constant in satellite BRFs.

To describe the relative rotational dynamics, let us assume the quaternion parameterization $\boldsymbol{q}_{C,T} = \boldsymbol{q}_e = [q_{e,0} \ \bar{\boldsymbol{q}}_e] = [q_{e,0} \ q_{e,1} \ q_{e,2} \ q_{e,3}]$ to represent the relative attitude between the chaser and target BRFs, such that

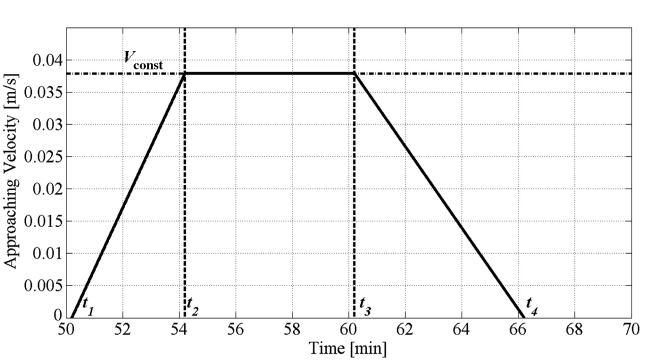

Fig. 2 Velocity profile for straight line trajectory.

$$\boldsymbol{q}_e = \begin{Bmatrix} q_{0,e} \\ \{\bar{\boldsymbol{q}}_e\} \end{Bmatrix} = \boldsymbol{q}_T^{-1} \otimes \boldsymbol{q}_C = \begin{bmatrix} q_{0,T}q_{0,C} + \{\bar{\boldsymbol{q}}_T\}^T\{\bar{\boldsymbol{q}}_C\} \\ q_{0,T}\{\bar{\boldsymbol{q}}_C\} - q_{0,C}\{\bar{\boldsymbol{q}}_T\} - [\bar{\boldsymbol{q}}_T\wedge]\bar{\boldsymbol{q}}_C \end{bmatrix} \tag{44}$$

where the symbol "⊗" denotes the quaternion product. Accordingly, the relative kinematics can be written as

$$\begin{aligned} \dot{\boldsymbol{q}}_e = \begin{Bmatrix} \dot{q}_{0,e} \\ \dot{\bar{\boldsymbol{q}}}_e \end{Bmatrix} &= \frac{1}{2}\begin{bmatrix} 0 & -\{\boldsymbol{\omega}_{C,T}^C\}^T \\ \{\boldsymbol{\omega}_{C,T}^C\} & [\boldsymbol{\omega}_{C,T}^C\wedge] \end{bmatrix}\boldsymbol{q}_e \\ &= \frac{1}{2}\begin{bmatrix} -\bar{\boldsymbol{q}}_e \\ q_{0,e}I_{3\times3} + [\bar{\boldsymbol{q}}_e\wedge] \end{bmatrix}\boldsymbol{\omega}_{C,T}^C \\ &= \frac{1}{2}\begin{bmatrix} -\bar{\boldsymbol{q}}_e \\ q_{0,e}I_{3\times3} + [\bar{\boldsymbol{q}}_e\wedge] \end{bmatrix}\boldsymbol{\omega}_{C,I}^C \\ &\quad -\frac{1}{2}\begin{bmatrix} 0 & -\{S_T^C(\boldsymbol{q}_e)\boldsymbol{\omega}_{T,I}^T\}^T \\ \{S_T^C(\boldsymbol{q}_e)\boldsymbol{\omega}_{T,I}^T\} & -[S_T^C(\boldsymbol{q}_e)\boldsymbol{\omega}_{T,I}^T\wedge] \end{bmatrix}\boldsymbol{q}_e \end{aligned} \tag{45}$$

The relative angular velocity between the chaser and target BRFs expressed in C is given by

$$\boldsymbol{\omega}_{C,T}^C = \boldsymbol{\omega}_{C,I}^C - S_T^C(\boldsymbol{q}_e)\boldsymbol{\omega}_{T,I}^T \tag{46}$$

where $S_T^C(\boldsymbol{q}_e)$ is the transformation matrix that describes the orientation of the C relative to the T and results [30]

$$S_T^C(\boldsymbol{q}_e) = \begin{bmatrix} q_{e,0}^2 + q_{e,1}^2 - q_{e,2}^2 - q_{e,3}^2 & 2(q_{e,1}q_{e,2} - q_{e,0}q_{e,3}) & 2(q_{e,1}q_{e,3} + q_{e,0}q_{e,2}) \\ 2(q_{e,1}q_{e,2} + q_{e,0}q_{e,3}) & q_{e,0}^2 - q_{e,1}^2 + q_{e,2}^2 - q_{e,3}^2 & 2(q_{e,2}q_{e,3} - q_{e,0}q_{e,1}) \\ 2(q_{e,1}q_{e,3} - q_{e,0}q_{e,2}) & 2(q_{e,2}q_{e,3} + q_{e,0}q_{e,1}) & q_{e,0}^2 - q_{e,1}^2 - q_{e,2}^2 + q_{e,3}^2 \end{bmatrix} \tag{47}$$

Thus, the time derivative of Eq. (46) leads to

$$\begin{aligned} \dot{\boldsymbol{\omega}}_{C,T}^C &= \dot{\boldsymbol{\omega}}_{C,I}^C - S_T^C(\boldsymbol{q}_e)\dot{\boldsymbol{\omega}}_{T,I}^T - \dot{S}_T^C(\boldsymbol{q}_e)\boldsymbol{\omega}_{T,I}^T \\ &= \dot{\boldsymbol{\omega}}_{C,I}^C - S_T^C(\boldsymbol{q}_e)\dot{\boldsymbol{\omega}}_{T,I}^T + [\boldsymbol{\omega}_{C,T}^C\wedge]S_T^C(\boldsymbol{q}_e)\boldsymbol{\omega}_{T,I}^T \end{aligned} \tag{48}$$

By using Eqs. (42) and (43), Eq. (48) can be rewritten as

$$\begin{aligned} \dot{\boldsymbol{\omega}}_{C,T}^C &= I_C^{-1}(-[(\boldsymbol{\omega}_{C,T}^C + S_T^C(\boldsymbol{q}_e)\boldsymbol{\omega}_{T,I}^T)\wedge]I_C(\boldsymbol{\omega}_{C,T}^C + S_T^C(\boldsymbol{q}_e)\boldsymbol{\omega}_{T,I}^T) + \boldsymbol{T}_{\text{ext}}^C) \\ &= -S_T^C(\boldsymbol{q}_e)(I_T^{-1}(-[\boldsymbol{\omega}_{T,I}^T\wedge]I_T\boldsymbol{\omega}_{T,I}^T + \boldsymbol{T}_{\text{ext}}^T)) - [S_T^C(\boldsymbol{q}_e)\boldsymbol{\omega}_{T,I}^T\wedge]\boldsymbol{\omega}_{C,T}^C \end{aligned} \tag{49}$$

Note that, in our work, only the disturbing torques due to the gravitational field are considered, such that the terms $\boldsymbol{T}_{\text{ext}}^C$ and $\boldsymbol{T}_{\text{ext}}^T$ reported in Eq. (49) become

$$\begin{aligned} \boldsymbol{T}_{\text{ext}}^C &= \boldsymbol{T}_{\text{grav}}^C + \boldsymbol{T}_{\text{control}}^C = 3\frac{\mu}{\|\boldsymbol{r}_C^C\|^5}[\boldsymbol{r}_C^C\wedge]I_C\boldsymbol{r}_C^C + \boldsymbol{T}_{\text{control}}^C \\ \boldsymbol{T}_{\text{ext}}^T &= \boldsymbol{T}_{\text{grav}}^T = 3\frac{\mu}{\|\boldsymbol{r}_T^T\|^5}[\boldsymbol{r}_T^T\wedge]I_T\boldsymbol{r}_T^T \end{aligned} \tag{50}$$

B. Extended Linearization of Coupled Relative Dynamics

As discussed in Sec. II, the SDRE controller requires one to bring the nonlinear dynamics equations to the SDC form. In light of this, Eqs. (41–45) can be represented in a compact form as follows:

$$\begin{aligned} \begin{bmatrix} \dot{\boldsymbol{\rho}}^H \\ \ddot{\boldsymbol{\rho}}^H \\ \dot{\boldsymbol{\omega}}_{C,I}^C \\ \dot{\boldsymbol{q}}_e \end{bmatrix} &= \begin{bmatrix} [0]_{3\times3} & [I]_{3\times3} & [0]_{3\times3} & [0]_{3\times4} \\ A_{\dot{\rho}\rho} & A_{\dot{\rho}\dot{\rho}} & [0]_{3\times3} & [0]_{3\times4} \\ A_{\omega\rho} & [0]_{3\times3} & A_{\omega\omega} & [0]_{3\times4} \\ [0]_{4\times3} & [0]_{4\times3} & A_{q\omega} & A_{qq} \end{bmatrix}\begin{bmatrix} \boldsymbol{\rho}^H \\ \dot{\boldsymbol{\rho}}^H \\ \boldsymbol{\omega}_{C,I}^C \\ \boldsymbol{q}_e \end{bmatrix} \\ &\quad + \begin{bmatrix} [0]_{3\times1} \\ [0]_{3\times1} \\ \{\boldsymbol{A}_{\omega\rho,\text{bias}}\} \\ [0]_{4\times1} \end{bmatrix} + \begin{bmatrix} [0]_{3\times3} & [0]_{3\times3} \\ [I]_{3\times3} & [0]_{3\times3} \\ [0]_{3\times3} & I_C^{-1} \\ [0]_{4\times3} & [0]_{4\times3} \end{bmatrix}\begin{bmatrix} \boldsymbol{f}_{\text{control},C}^H \\ \boldsymbol{T}_{\text{control},C}^C \end{bmatrix} \end{aligned}$$

$$A_{\dot{\rho}\rho} = -[\boldsymbol{\omega}_{H,I}^H\wedge][\boldsymbol{\omega}_{H,I}^H\wedge] + [\dot{\boldsymbol{\omega}}_{H,I}^H\wedge] + \mu\left(\frac{(r_C^2 + r_Tr_C + r_T^2)}{r_T^2r_C^3(r_T + r_C)}\right)\begin{bmatrix} 2r_T + x & y & z \\ 0 & 0 & 0 \\ 0 & 0 & 0 \end{bmatrix} - \frac{\mu}{r_C^3}[I]_{3\times3}$$

$$A_{\omega\rho} = \frac{3\mu}{r_C^5}I_C^{-1}([S_T^CS_H^T\boldsymbol{r}_T^H\wedge]I_CS_T^C + [S_T^CS_H^T\boldsymbol{\rho}^H\wedge]I_CS_T^C - [I_CS_T^CS_H^T\boldsymbol{\rho}^H\wedge]S_T^C)$$

$$A_{\omega\omega} = I_C^{-1}(-[\boldsymbol{\omega}_{C,I}^C\wedge]I_C\boldsymbol{\omega}_{C,I}^C)$$

$$A_{\dot{\rho}\dot{\rho}} = -2[\boldsymbol{\omega}_{H,I}^H\wedge]$$

$$A_{q\omega} = \frac{1}{2}\begin{bmatrix} -\bar{\boldsymbol{q}}_e \\ q_{0,e}I_{3\times3} + [\bar{\boldsymbol{q}}_e\wedge] \end{bmatrix}$$

$$A_{qq} = -\frac{1}{2}\begin{bmatrix} 0 & -\{S_T^C(\boldsymbol{q}_e)\boldsymbol{\omega}_{T,I}^T\}^T \\ \{S_T^C(\boldsymbol{q}_e)\boldsymbol{\omega}_{T,I}^T\} & -[S_T^C(\boldsymbol{q}_e)\boldsymbol{\omega}_{T,I}^T\wedge] \end{bmatrix}$$

$$\{\boldsymbol{A}_{\omega\rho,\text{bias}}\} = \frac{3\mu}{r_C^5}I_C^{-1}([S_T^CS_H^T\boldsymbol{r}_T^H\wedge]I_CS_T^CS_H^T\boldsymbol{r}_T^H) \tag{51}$$

It is worth noting that the state-independent term in Eq. (51) $\boldsymbol{A}_{\omega\rho,\text{bias}}$, referred to as the bias term, will have to be handled to conform the dynamic system to the basic structure and conditions required for the straightforward application of the SDRE method (i.e., conditions 1 and 2 mentioned in Sec. II). In accordance with the techniques proposed in [31] to handle the bias terms, a new stable state s is added such that Eq. (51) becomes

$$\begin{aligned} \begin{bmatrix} \dot{\boldsymbol{\rho}}^H \\ \ddot{\boldsymbol{\rho}}^H \\ \dot{s} \\ \dot{\boldsymbol{\omega}}_{C,I}^C \\ \dot{\boldsymbol{\rho}}_e \end{bmatrix} &= \begin{bmatrix} [0]_{3\times3} & [I]_{3\times3} & [0]_{3\times1} & [0]_{3\times3} & [0]_{3\times4} \\ A_{\dot{\rho}\rho} & A_{\dot{\rho}\dot{\rho}} & [0]_{3\times1} & [0]_{3\times3} & [0]_{3\times4} \\ [0]_{1\times3} & [0]_{1\times3} & -\lambda_s & [0]_{1\times3} & [0]_{1\times4} \\ A_{\omega\rho} & [0]_{3\times3} & \{\boldsymbol{A}_{\omega s}\} & A_{\omega\omega} & [0]_{3\times4} \\ [0]_{4\times3} & [0]_{4\times3} & [0]_{4\times1} & A_{q\omega} & A_{qq} \end{bmatrix}\begin{bmatrix} \boldsymbol{\rho}^H \\ \dot{\boldsymbol{\rho}}^H \\ s \\ \boldsymbol{\omega}_{C,I}^C \\ \boldsymbol{\rho}_e \end{bmatrix} \\ &\quad + \begin{bmatrix} [0]_{3\times3} & [0]_{3\times3} \\ [I]_{3\times3} & [0]_{3\times3} \\ [0]_{1\times3} & [0]_{1\times3} \\ [0]_{3\times3} & I_C^{-1} \\ [0]_{4\times3} & [0]_{4\times3} \end{bmatrix}\begin{bmatrix} \boldsymbol{f}_{\text{control},C}^H \\ \boldsymbol{T}_{\text{control}}^C \end{bmatrix} \end{aligned}$$

$$\{\boldsymbol{A}_{\omega s}\} = \frac{1}{s}[I]_{3\times3}\{\boldsymbol{A}_{\omega\rho,\text{bias}}\} \tag{52}$$

where λ_s is a small positive number.

V. Guidance Law for Rendezvous and Docking Maneuver

The guidance law defines the set values for the nominal evolution of the chaser satellite state, that is, the references for the control of relative position, velocity, attitude, and angular rates at each point in time [1]. More specifically, in our study, we consider an approaching trajectory consisting of a V hop and a straight line along the V-bar direction [32,33]. [In R&D literature, the V-bar versor is oriented as the velocity vector, the H-bar versor is aligned with the zenith direction, and the R-bar versor is directed along the opposite direction of the angular momentum vector of the target orbit. This reference frame is known as the local vertical/local horizontal frame.] The reference relative position and relative velocity for the hopping phase is provided by the analytical solution of Hill–Clohessy–Wiltshire (HCW) equations; particularly, if we define the initial reference relative position $\boldsymbol{\rho}^H_{\text{ref}}(0)$ and the time interval to perform the V-hop maneuver $\mathrm{d}t_{\text{V-hop}}$, the translational reference state $\boldsymbol{x}_{\text{trans,ref}}(t) = [\boldsymbol{\rho}^H_{\text{ref}}(t) \quad \dot{\boldsymbol{\rho}}^H_{\text{ref}}(t)]^T$ can be determined as follows:

$$\begin{bmatrix} \boldsymbol{\rho}^H_{\text{ref}}(t) \\ \dot{\boldsymbol{\rho}}^H_{\text{ref}}(t) \end{bmatrix} = [\Phi(t)] \begin{bmatrix} \boldsymbol{\rho}^H_{\text{ref}}(0) \\ \dot{\boldsymbol{\rho}}^H_{\text{ref}}(0) \end{bmatrix}; \qquad \Phi(t) = \begin{bmatrix} [M(t)] & [N(t)] \\ [S(t)] & [T(t)] \end{bmatrix} \tag{53}$$

$$M(t) = \begin{bmatrix} 4-3\cos(\omega_z \mathrm{d}t_{\text{V-hop}}) & 0 & 0 \\ 6(\sin(\omega_z \mathrm{d}t_{\text{V-hop}}) - \omega_z \mathrm{d}t_{\text{V-hop}}) & 1 & 0 \\ 0 & 0 & \cos(\omega_z \mathrm{d}t_{\text{V-hop}}) \end{bmatrix}$$

$$N(t) = \begin{bmatrix} \frac{\sin(\omega_z \mathrm{d}t_{\text{V-hop}})}{\omega_z} & \frac{2}{\omega_z}(1-\cos(\omega_z \mathrm{d}t_{\text{V-hop}})) & 0 \\ -\frac{2}{\omega_z}(1-\cos(\omega_z \mathrm{d}t_{\text{V-hop}})) & \frac{4\sin(\omega_z \mathrm{d}t_{\text{V-hop}}) - 3(\omega_z \mathrm{d}t_{\text{V-hop}})}{\omega_z} & 0 \\ 0 & 0 & \frac{\sin(\omega_z \mathrm{d}t_{\text{V-hop}})}{\omega_z} \end{bmatrix} \tag{54}$$

$$S(t) = \begin{bmatrix} 3\omega_z \sin(\omega_z \mathrm{d}t_{\text{V-hop}}) & 0 & 0 \\ -6\omega_z(1-\cos(\omega_z \mathrm{d}t_{\text{V-hop}})) & 0 & 0 \\ 0 & 0 & -\omega_z \sin(\omega_z \mathrm{d}t_{\text{V-hop}}) \end{bmatrix}$$

$$T(t) = \begin{bmatrix} \cos(\omega_z \mathrm{d}t_{\text{V-hop}}) & 2\sin(\omega_z \mathrm{d}t_{\text{V-hop}}) & 0 \\ -2\sin(\omega_z \mathrm{d}t_{\text{V-hop}}) & 4\cos(\omega_z \mathrm{d}t_{\text{V-hop}}) - 3 & 0 \\ 0 & 0 & \cos(\omega_z \mathrm{d}t_{\text{V-hop}}) \end{bmatrix}$$

$$\dot{\boldsymbol{\rho}}^H_{\text{ref}}(0) = N(\mathrm{d}t_{\text{V-hop}})^{-1}(\boldsymbol{\rho}^H_{\text{ref}}(\mathrm{d}t_{\text{V-hop}}) - M(\mathrm{d}t_{\text{V-hop}})\boldsymbol{\rho}^H_{\text{ref}}(0)) \tag{55}$$

where $\omega_z = \boldsymbol{\omega}^H_{H,I} \cdot \hat{\boldsymbol{h}}$. Let us recall that the HCW equations are based on the assumptions of circular target orbit and small relative radius with respect to the distance of the target satellite from Earth center ($\|\boldsymbol{\rho}\| \ll \|\boldsymbol{r}_T\|$) [34].

For what concerns the final approach, a specific velocity profile is implemented along the V-bar direction, whereas velocity components along other directions are zero (see Fig. 2). A constant acceleration is considered at the start of forced motion to achieve a desired approach velocity V_{const} in a fixed interval time $\mathrm{d}t_1 = t_2 - t_1$; correspondingly, at the end, a constant deceleration is implemented to achieve the desired relative position and velocity in a fixed interval time $\mathrm{d}t_3 = t_4 - t_3$ [1]. The desired velocity V_{const} is given by

$$V_{\text{const}} = \frac{2(\rho_{y,\text{desired}}(t_4) - \rho_{y,\text{desired}}(t_1))}{t_4 + t_3 - t_2 - t_1} \tag{56}$$

Finally, to guarantee the docking port of target faces the chaser one, the satellites' angular velocities must be equal and the axes of satellites' BRFs must be aligned during the whole approaching maneuver. Defining the reference rotational state as $\boldsymbol{x}_{\text{rot,ref}}(t) = [\boldsymbol{\omega}^C_{C,I\text{ref}}(t) \quad \boldsymbol{q}_{e,\text{ref}}(t)]^T$, it yields

$$\begin{bmatrix} \boldsymbol{\omega}^C_{C,I\text{ref}}(t) \\ \boldsymbol{q}_{e,\text{ref}}(t) \end{bmatrix} = \begin{bmatrix} S^C_T(\boldsymbol{q}_e)\boldsymbol{\omega}^T_{T,I}(t) \\ [1 \quad 0 \quad 0 \quad 0]^T \end{bmatrix} \tag{57}$$

VI. Experimental Test Bed

The test bed designed by DLR Institute of Space Systems, referred to as the Test Environment for Application of Multiple Spacecraft (TEAMS), consists of a granite table (4×5 m) with several air cushion vehicles moving on it [35]. Each vehicle floats thanks to a set of air bearing pads, reproducing a frictionless and weightless environment in two dimensions and three degrees of freedom. The table surface is manufactured with an accuracy of 3 μm and leveled with an accuracy of less than 20 μm from an edge to another to keep the gravitational field disturbances low. The thickness of the granite is 60 cm, a value necessary to keep the high evenness in presence of the load due to the air cushion vehicles and the granite table's own weight.

The air cushion vehicles consist of two parts (see Fig. 3). The lower part, referred to as the transport platform (TP), is devoted to contain the air tanks and the pressure regulators to support the pads and proportional thrusters with pressurized air. On the top of the TP, the second stage, referred to as the attitude platform (AP), is constrained such that no relative motion between two parts is permitted. On the AP, the sensors, actuators, and electronic equipment are located such that the position of the center of mass of the vehicle is not far from the junction point of the two stages.

To measure the position and attitude of the vehicles, an infrared indoor system (DTrack) is exploited. It consists mainly of three elements: 1) a dedicated tracking PC; 2) a set of six cameras; and 3) five target markers installed on each floating vehicle. The cameras emit infrared flashes with a frequency of 60 Hz, which are reflected by a set of reflective balls (markers) installed onboard the vehicle; the reflected signal is captured by the cameras and handled by the tracking PC, which computes the navigation solution and, subsequently, broadcasts it on the local network.

The AP is equipped with six proportional thrusters consisting of a proportional valve and a nozzle designed for this specific application. The valves are controlled by a pulse-width modulation signal, which is generated by a microcontroller on a separate thruster control board and can provide a maximum thrust of 65 mN. The onboard computer is a PC104 stack equipped by an x86 Atom Z530 processor with 1.6 GHz and several boards for program upload, commanding, and data download. It is provided by the real-time operating system QNX. The development of control/estimation applications is based on the MATLAB/Simulink environment: After designing the onboard algorithms with Simulink, the model is converted to C code using Real-Time Workshop and compiled using the QNX C compiler; finally, the executable file is uploaded, to the onboard computer via Wireless Local Area Network and executed.

Note that the vehicles are completely autonomous: The onboard computer calculates the control solution by using DTrack data and sends the commands to the thrusters' control board; the power distribution unit supplies all electronics components.

VII. Orbital Motion Simulation on the Testbed

To emulate the orbital dynamics of the chaser satellite relative to the Hill reference frame by using the presented test bed, it is necessary that the vehicle actuator system generates the inertia acceleration/torque due to the orbital motion of the Hill reference frame and the gravitational force/torque, besides the control signal. Moreover, both the provided inertia and control acceleration/torque have to be scaled to satisfy the facility constraints.

For sake of clarity, let us derive the equations of motion of the vehicle moving on the frictionless surface as (see Fig. 4),

$$\begin{aligned} \ddot{\boldsymbol{r}}^{\text{HT}}_V &= \boldsymbol{f}^{\text{HT}}_{\text{Thrust}} \\ \dot{\boldsymbol{\omega}}^V_{V,\text{HT}} &= I_V^{-1}(-[\boldsymbol{\omega}^V_{V,\text{HT}} \wedge] I_V \boldsymbol{\omega}^{\text{HT}}_{V,\text{HT}} + \boldsymbol{T}^V_{\text{Thrust}}) \end{aligned} \tag{58}$$

Note that the coordinate system denoted as HT in Fig. 4 represents the Hill reference frame or the noninertial reference frame R (see

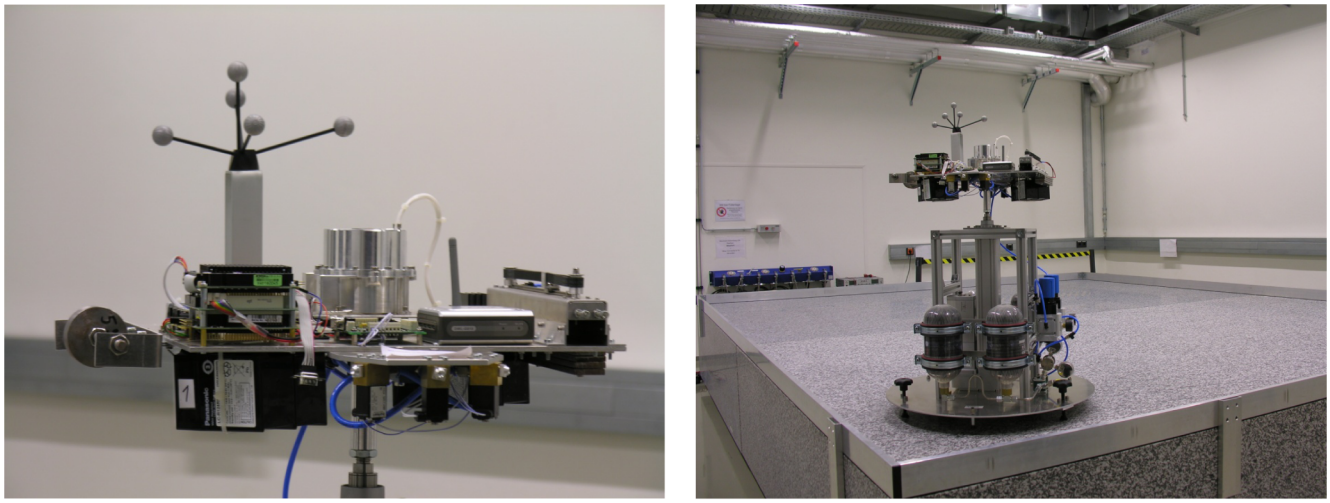

a) b)

Fig. 3 TEAMS platform: a) AP detailed overview; b) assembled vehicle configuration.

Sec. VIII for more details). So that dynamics Eqs. (58) correspond to the Eqs. (41–49), the terms $\boldsymbol{f}^{\mathrm{HT}}_{\mathrm{Thrust}}$ and $\boldsymbol{T}^{V}_{\mathrm{Thrust}}$ must to be set to

$$
\begin{aligned}
\boldsymbol{f}^{\mathrm{HT}}_{\mathrm{Thrust}} &= -[\dot{\check{\boldsymbol{\omega}}}^{H}_{H,I}\wedge]\check{\boldsymbol{\rho}}^{H} - 2[\check{\boldsymbol{\omega}}^{H}_{H,I}\wedge]\dot{\check{\boldsymbol{\rho}}}^{H} - [\check{\boldsymbol{\omega}}^{H}_{H,I}\wedge][\check{\boldsymbol{\omega}}^{H}_{H,I}\wedge]\check{\boldsymbol{\rho}}^{H} \\
&\quad + \check{\boldsymbol{f}}^{C}_{\mathrm{grav},C} - \check{\boldsymbol{f}}^{T}_{\mathrm{grav},T} + \check{\boldsymbol{f}}^{H}_{\mathrm{control},C} \\
\boldsymbol{T}^{V}_{\mathrm{Thrust}} &= I_V(\check{I}^{-1}_{C}(-[\check{\boldsymbol{\omega}}^{C}_{C,I}\wedge]\check{I}_{C}\check{\boldsymbol{\omega}}^{C}_{C,I} + \check{\boldsymbol{T}}^{C}_{\mathrm{grav}}) - S^{C}_{H}\dot{\check{\boldsymbol{\omega}}}^{H}_{H,I} \\
&\quad - [S^{C}_{H}\check{\boldsymbol{\omega}}^{H}_{H,I}\wedge]\check{\boldsymbol{\omega}}^{C}_{C,H}) + [\boldsymbol{\omega}^{V}_{V,\mathrm{HT}}\wedge]I_V\boldsymbol{\omega}^{V}_{V,\mathrm{HT}} + I_V\check{I}^{-1}_{C}\check{\boldsymbol{T}}^{C}_{\mathrm{control}} \\
\check{\boldsymbol{f}}^{C}_{\mathrm{grav},C} &= -\frac{\check{\mu}}{\|\check{\boldsymbol{r}}^{H}_{T} + \check{\boldsymbol{\rho}}^{H}\|^{3}}(\check{\boldsymbol{r}}^{H}_{T} + \check{\boldsymbol{\rho}}^{H}) \\
\check{\boldsymbol{f}}^{T}_{\mathrm{grav},T} &= -\frac{\check{\mu}}{\|\check{\boldsymbol{r}}^{H}_{T}\|^{3}}(\check{\boldsymbol{r}}^{H}_{T}) \\
\check{\boldsymbol{T}}^{C}_{\mathrm{grav}} &= -\frac{\check{\mu}}{\|\check{\boldsymbol{r}}^{H}_{T} + \check{\boldsymbol{\rho}}^{H}\|^{5}}[(\check{\boldsymbol{r}}^{H}_{T} + \check{\boldsymbol{\rho}}^{H})\wedge]\check{I}^{C}(\check{\boldsymbol{r}}^{H}_{T} + \check{\boldsymbol{\rho}}^{H})
\end{aligned}
\tag{59}
$$

where the superscript $\check{}$ indicates the scaled variable. From Eq. (59), it is evident that Eqs. (58) coincide with Eqs. (41–49) if

$$
\check{\boldsymbol{\rho}}^{H} = \boldsymbol{r}^{\mathrm{HT}}_{V} \qquad \dot{\check{\boldsymbol{\rho}}}^{H} = \boldsymbol{r}^{\mathrm{HT}}_{V} \qquad \check{\boldsymbol{\omega}}^{C}_{C,H} = \boldsymbol{\omega}^{V}_{V,\mathrm{HT}} \qquad \check{\boldsymbol{q}}_{e} = \boldsymbol{q}_{V,\mathrm{HT}} \tag{60}
$$

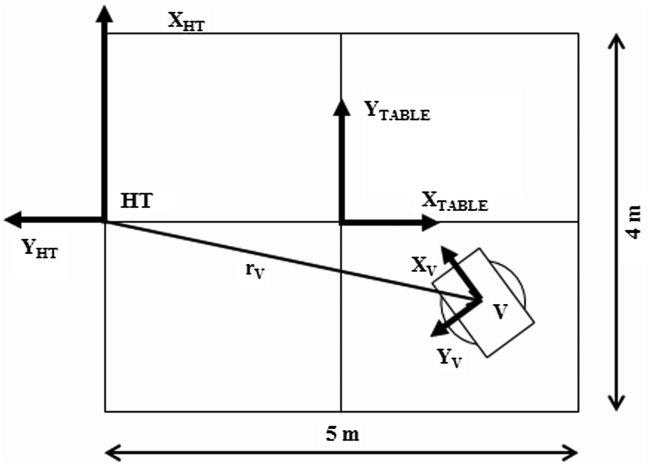

Fig. 4 Layout of testbed.

and

$$
\begin{aligned}
&\check{\boldsymbol{\rho}}^{H} = \boldsymbol{\rho}^{H}l \qquad \dot{\check{\boldsymbol{\rho}}}^{H} = \dot{\boldsymbol{\rho}}^{H}l/t \\
&\check{\boldsymbol{\omega}}^{C}_{C,H} = \boldsymbol{\omega}^{C}_{C,H}/t \qquad \dot{\check{\boldsymbol{\omega}}}^{C}_{C,H} = \dot{\boldsymbol{\omega}}^{C}_{C,H}/t^{2} \qquad \check{\boldsymbol{\omega}}^{H}_{H,I} = \boldsymbol{\omega}^{H}_{H,I}/t \\
&\check{I}_{C} = I_{C}kl^{2} \qquad \check{\mu} = \mu l^{3}/t^{2}
\end{aligned}
\tag{61}
$$

where l, t, and k are length, time, and mass scale factors defined such that 1) the maximum scaled relative position does not overcome the frictionless surface dimension; 2) the vehicle completes the maneuver within the maximum autonomy time (i.e., the time needed to empty the air pressurized tanks and to discharge the onboard batteries); and 3) the scaled chaser satellite mass is equal to the floating vehicle mass.

Note that, in our experiments, a docking maneuver is emulated assuming that the target satellite motion is known by the chaser.

VIII. Simulated Scenario

The main purpose of the experimental campaigns is to prove the effectiveness of new proposed DA-based algorithm. Particularly, two maneuvers are simulated by using the TEAMS platform: 1) close range R&D maneuver; 2) final approach to dock a tumbling target.

During the close-range R&D maneuver, the target satellite is assumed to be controlled such that its orbital motion is Keplerian and its BRF is oriented as the Hill reference frame. More specifically, we assume that the target satellite is moving on a circular orbit at $r_T = 400$ km from the Earth surface, such that $\boldsymbol{\omega}^{H}_{H,I} = [0 \quad 0 \quad \sqrt{\mu/r_T^3}]$ and $\boldsymbol{r}^{H}_{T} = [r_T \quad 0 \quad 0]$. Furthermore, the chaser satellite has to approach the target tracking a specific trajectory consisting of one V-hop and a V-bar forced motion and provide the right attitude, allowing docking with the target, as discussed in Sec. V. A maximum range of 100 m is considered. During the final approach maneuver, the target satellite tumbles and moves with respect to a noninertial reference frame R, which orbits around the Earth at $r_R = 400$ km km with a constant angular velocity $\boldsymbol{\omega}^{R}_{R,I} = [0 \quad 0 \quad \sqrt{\mu/r_T^3}]$. As illustrated in Fig. 5, the aforementioned coordinate system has the x axis aligned with the radial direction and the z axis orthogonal to the orbit plane. The target spacecraft motion is known and given by the integration of the following dynamic equations:

$$
\begin{aligned}
\ddot{\boldsymbol{r}}^{R}_{T,R} &= -2[\boldsymbol{\omega}^{H}_{H,I}\wedge]\dot{\boldsymbol{r}}^{R}_{T,R} - [\boldsymbol{\omega}^{R}_{R,I}\wedge][\boldsymbol{\omega}^{R}_{R,I}\wedge]\boldsymbol{r}^{R}_{T,R} - [\dot{\boldsymbol{\omega}}^{R}_{R,I}\wedge]\boldsymbol{r}^{R}_{T,R} \\
&\quad + \frac{\mu}{\|\boldsymbol{r}^{R}_{R} + \boldsymbol{r}^{R}_{T,R}\|^{3}}(\boldsymbol{r}^{R}_{R} + \boldsymbol{r}^{R}_{T,R}) + \frac{\mu}{\|\boldsymbol{r}^{R}_{R}\|^{3}}(\boldsymbol{r}^{R}_{R})
\end{aligned}
\tag{62}
$$

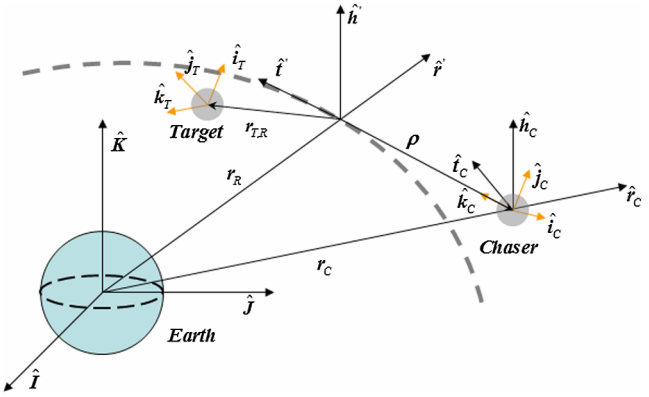

Fig. 5 Supporting noninertial reference frame $R = \{\hat{r}' \quad \hat{t}' \quad \hat{h}'\}$.

$$\dot{\boldsymbol{\omega}}_{T,R}^{T} = I_T^{-1}(-[(\boldsymbol{\omega}_{T,R}^{T} + S_R^T(\boldsymbol{q}_{T,R})\boldsymbol{\omega}_{R,I}^{R})\wedge]I_C(\boldsymbol{\omega}_{T,R}^{T} + S_R^T(\boldsymbol{q}_{T,R})\boldsymbol{\omega}_{R,I}^{R}) + \boldsymbol{T}_{\text{grav}}^{T}) - [S_R^T(\boldsymbol{q}_{T,R})\boldsymbol{\omega}_{R,I}^{R}\wedge]\boldsymbol{\omega}_{T,R}^{T} \tag{63}$$

$$\dot{\boldsymbol{q}}_{T,R} = \begin{Bmatrix} \dot{q}_{0,T,R} \\ \dot{\tilde{\boldsymbol{q}}}_{T,R} \end{Bmatrix} = \frac{1}{2}\begin{bmatrix} 0 & -\{\boldsymbol{\omega}_{T,R}^{T}\}^T \\ \{\boldsymbol{\omega}_{T,R}^{T}\} & [\boldsymbol{\omega}_{T,R}^{T}\wedge] \end{bmatrix}\boldsymbol{q}_{T,R} \tag{64}$$

with following initial conditions

$$\begin{aligned} \boldsymbol{r}_{T,R}^{R}(0) &= [0 \quad 0 \quad 0]^T \text{ m} \\ \dot{\boldsymbol{r}}_{T,R}^{R}(0) &= [-0.0026 \quad 0.0022 \quad 0] \text{ m/s} \\ \boldsymbol{q}_{T,R}(0) &= [1 \quad 0 \quad 0 \quad 0]^T \\ \boldsymbol{\omega}_{T,R}^{T}(0) &= [0 \quad 0 \quad 0.0017] \text{ rad/s} \end{aligned} \tag{65}$$

Finally, the chaser has to approach the uncontrolled target by following a trapezoidal velocity profile along the versor $-\hat{\boldsymbol{j}}_T$ of the target BRF, as discussed in Sec. V. A short range of 5 m is considered.

In the following subsections, the experimental results regarding the preceding orbital maneuvers are presented. Let us note that only one vehicle is used to simulate the aforementioned maneuvers, that is, the motion of the target is numerically simulated by the TEAMS vehicle onboard computer, whenever it is necessary; actually, this fact does not invalidate our study, which aims at analyzing the performance of the DA-based controller for the approach maneuvering rather than to investigate such phenomena as contact dynamics or docking mechanism functionality. Moreover, let us note that the DTrack system provides only the relative position and attitude of the TEAMS vehicle; thus, the extended Kalman filter (EKF) based on the linearized form of Eqs. (41–48) is implemented to estimate the relative velocity $\breve{\boldsymbol{\rho}}^H$ and the angular rate $\breve{\boldsymbol{\omega}}_{C/I}^{C}$ [35]. [The DTrack system provides the position and the attitude of the vehicle with respect to the table reference frame placed in the center of the table (see Fig. 4). However, the position and the attitude of the vehicle relative to the HT reference frame can be easily computed by a rototranslation transformation.]

IX. Results

In this section, the experimental results concerning the two R&D maneuvers presented in Sec. VIII will be shown. Particularly, the performance of the Newton and DA-based algorithms for the solution of the SDRE controller will be discussed, assuming a maximum number of five iterations for the NM approach and a third-order Taylor expansion v for the DA-based algorithm. For sake of clarity only the results due to the DA-based will be illustrated.

Note that, because the controller has to track a specific reference signal $\boldsymbol{x}_{\text{ref}}$, the control law described by Eq. (32) becomes

$$\begin{aligned} \boldsymbol{U}_{\text{SDRE/DA}}^{(3)}(\delta\boldsymbol{x}) &= -Z^{-1}(B_0 + \Delta B(\delta\boldsymbol{x}))^T\left(\sum_{k=0}^{l} P_k(\delta\boldsymbol{x})\right)\delta\boldsymbol{x} \\ &= \tilde{K}(\delta\boldsymbol{x})\delta(\boldsymbol{x} - \boldsymbol{x}_{\text{ref}}) = -Z^{-1}(B_0 + \Delta B(\delta\boldsymbol{x}))^T\left(\sum_{k=0}^{l} P_k(\delta\boldsymbol{x})\right)\delta\boldsymbol{x} \\ &= \tilde{K}(\delta\boldsymbol{x})(\delta\boldsymbol{x} - \delta\boldsymbol{x}_{\text{ref}}) \end{aligned} \tag{66}$$

where

$$\begin{aligned} \delta\boldsymbol{x} &= [\delta\breve{\boldsymbol{\rho}}^H \quad \delta\dot{\breve{\boldsymbol{\rho}}}^H \quad \delta s \quad \delta\breve{\boldsymbol{\omega}}_{C,I}^{C} \quad \delta\breve{\boldsymbol{q}}_e] \\ \delta\boldsymbol{x}_{\text{ref}} &= [\delta\breve{\boldsymbol{\rho}}_{\text{ref}}^H \quad \delta\dot{\breve{\boldsymbol{\rho}}}_{\text{ref}}^H \quad \delta s_{\text{ref}} \quad \breve{\boldsymbol{\omega}}_{C,I\text{ref}}^{C} \quad \delta\breve{\boldsymbol{q}}_{e\text{ref}}] \end{aligned} \tag{67}$$

represent the deviation from reference vectors

$$\begin{aligned} \boldsymbol{x}^0 &= [\breve{\boldsymbol{\rho}}^{0H} \quad \dot{\breve{\boldsymbol{\rho}}}^{0H} \quad \delta s^0 \quad \breve{\boldsymbol{\omega}}_{C,I}^{0C} \quad \breve{\boldsymbol{q}}_e^0] \\ &= [[0]_{1\times3} \quad [0]_{1\times3} \quad 1 \quad \breve{\boldsymbol{\omega}}_{H,I}^{H} \quad [1,0,0,0]] \\ \boldsymbol{x}_{\text{ref}}^0 &= [\breve{\boldsymbol{\rho}}_{\text{ref}}^{0H} \quad \dot{\breve{\boldsymbol{\rho}}}_{\text{ref}}^{0H} \quad \delta s_{\text{ref}}^0 \quad \breve{\boldsymbol{\omega}}_{C,I\text{ref}}^{0C} \quad \breve{\boldsymbol{q}}_{e,\text{ref}}^0] \\ &= [[0]_{1\times3} \quad [0]_{1\times3} \quad 1 \quad \breve{\boldsymbol{\omega}}_{H,I}^{H} \quad [1,0,0,0]] \end{aligned} \tag{68}$$

Finally, let us remark that the actuator system installed on TEAMS vehicle produces only the inertial and gravitational forces/torques, ignoring the forces/torques due to modeling the Earth oblateness and atmospheric drag effects. This choice is due to the order of magnitude of these scaled orbital perturbing effects; in fact they are smaller than the forces/torques due to the laboratory environment, such as the forces due to nonleveled frictionless surface or the torques due to offset between center of gravity and point of conjunction between the two stages of the vehicle.

A. Close Range R&D Maneuver

The length, time, and mass scale factors required to scale the control and the inertial and gravitational forces/torques for the TEAMS platform are $l = 0.04$, $t = 0.1877$, and $k = 0.046$, respectively. Note that these values are related to the vehicle mass, to the dimension of the arena where the TEAMS vehicle moves, and to the autonomy of the air pressured system.

As discussed in Sec. V, the reference trajectory consists of a V-bar hop and V-bar straight line and its sketch on a frictionless surface is depicted in Fig. 6. Accordingly, Table 1 reports the reference position vector corresponding with the main points of V-hop and forced motion expressed in the Hill reference frame and its scaled counterpart expressed in the table fixed reference frame. (The table fixed reference frame is centered in the center of the frictionless plane and has the z axis orthogonal to the table. The x and y axes lie on the plane as illustrated in Fig. 6.) Let us remark that the HT coordinate system represents the Hill reference frame and the virtual target vehicle is assumed fixed with respect to HT during the maneuver.

The entire orbital maneuver is simulated in 12 min; this is the time required by the air pressure tanks to be almost emptied. The SDRE/DA controller design is based on a scaled version of the unperturbed dynamic model (52) and it runs at 10 Hz. The weighting matrices Q and Z are positive definitive and constant, and they are set to

Table 1 Orbital range for R&D maneuver simulated by TEAMS facility

Reference trajectory	P_1, m	P_2, m	P_3, m
Reference position vector in the table reference frame	[2 0]	[−1.64 0]	[−1.8 0]
Reference position vector in H	[0 −100 0]	[0 −90 0]	[0 −5 0]

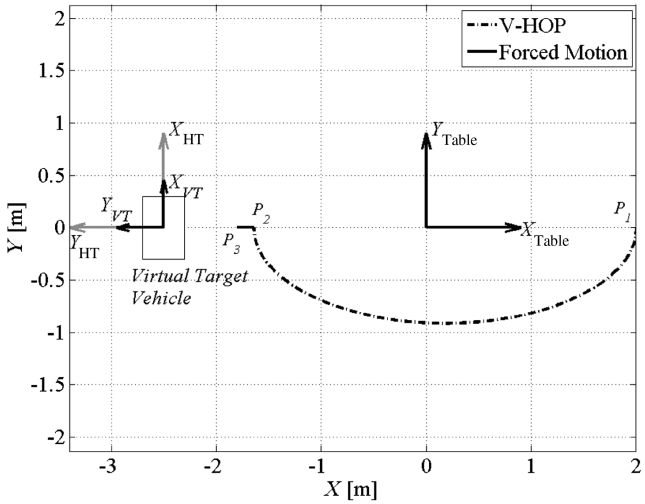

Fig. 6 Reference trajectory on frictionless surface.

$$Q = \text{diag}([\,Q_{11} \quad Q_{22} \quad 0 \quad Q_{33} \quad Q_{44}\,])$$
$$Z = \text{diag}([\,Z_{11} \quad Z_{22}\,])$$
$$Q_{11} = \text{diag}([\,1e-4 \quad 1e-4 \quad 1e-6\,])\ 1/\text{m}^2$$
$$Q_{22} = \text{diag}([\,10e-2 \quad 10e-2 \quad 10e-4\,])\ \text{s/m}^2$$
$$Q_{33} = [I]_{3\times3}1e-7\ \text{s}^2$$
$$Q_{44} = [I]_{4\times4}1e-7\ (\text{s}^2/\text{m})^2$$
$$Z_{11} = [I]_{3\times3}1.5\ (\text{s}^2/\text{m})^2$$
$$Z_{22} = \text{diag}([\,1e-4 \quad 1e-4 \quad 1e-8\,])\ (\text{s}^2/\text{kgm}^2)^2 \qquad (69)$$

Note that the preceding matrices have to be scaled according with length, time, and mass scale factors. Thus, for instance, the block Q_{11} has to be divided by square of length scale factor $l = 0.04$.

Figures 7 and 8 illustrate the relative position error, the relative velocity error, the absolute angular rate error, and the relative quaternion error regarding the TEAMS vehicle motion. The aforementioned errors represent the difference between the state estimated by the EKF $\boldsymbol{x}_{\text{Estimated}} = \left[\breve{\boldsymbol{\rho}}^H_{\text{Estimated}} \quad \dot{\breve{\boldsymbol{\rho}}}^H_{\text{Estimated}} \quad \breve{\boldsymbol{\omega}}^C_{C,I\text{Estimated}} \quad \breve{\boldsymbol{q}}_{e\text{Estimated}}\right]$, and reference one $\boldsymbol{x}_{\text{ref}} = \left[\breve{\boldsymbol{\rho}}^H_{\text{ref}} \quad \dot{\breve{\boldsymbol{\rho}}}^H_{\text{ref}} \quad \breve{\boldsymbol{\omega}}^C_{C,I\text{ref}} \quad \breve{\boldsymbol{q}}_{e\text{ref}}\right]$, such as

$$\boldsymbol{e} = [\boldsymbol{e}_\rho\ \boldsymbol{e}_{\dot\rho}\ \boldsymbol{e}_{\omega^C_{C/I}}\ \boldsymbol{e}_q]$$
$$= [\breve{\boldsymbol{\rho}}^H_{\text{Estimated}} - \breve{\boldsymbol{\rho}}^H_{\text{ref}}\ \dot{\breve{\boldsymbol{\rho}}}^H_{\text{Estimated}} - \dot{\breve{\boldsymbol{\rho}}}^H_{\text{ref}}\ \breve{\boldsymbol{\omega}}^C_{C,I\text{Estimated}} - \breve{\boldsymbol{\omega}}^C_{C,I\text{ref}}\ \breve{\boldsymbol{q}}_{e\text{Estimated}} - \breve{\boldsymbol{q}}_{e\text{ref}}] \qquad (70)$$

where the superscript $\breve{}$ indicates the scaled variable.

It is worth noting that the SDRE/DA controller guarantees the TEAMS floating vehicle to approach the virtual target vehicle following the defined trajectory; at the end of the maneuver, the norm of relative position error is about $8.84e-3$ m, whereas the norm of relative velocity error is about $1.12e-3$ m/s.

Note that the oscillation shown in the absolute angular velocity error and relative quaternion error plots at about 4.6 min is due to a gap on the granite table that blocks up the transition of one air pad, generating a disturbing torque. This phenomenon occurs randomly and it was not significant in many experiments; also in the presence of this environmental disturbing effect, the SDRE controller is able to nullify the relative attitude of the floating vehicle with respect to the virtual target vehicle, synchronizing the vehicles body-fixed reference frames. Moreover, the left side of Fig. 9 illustrates the scaled force and torque expressed in the table coordinate system and

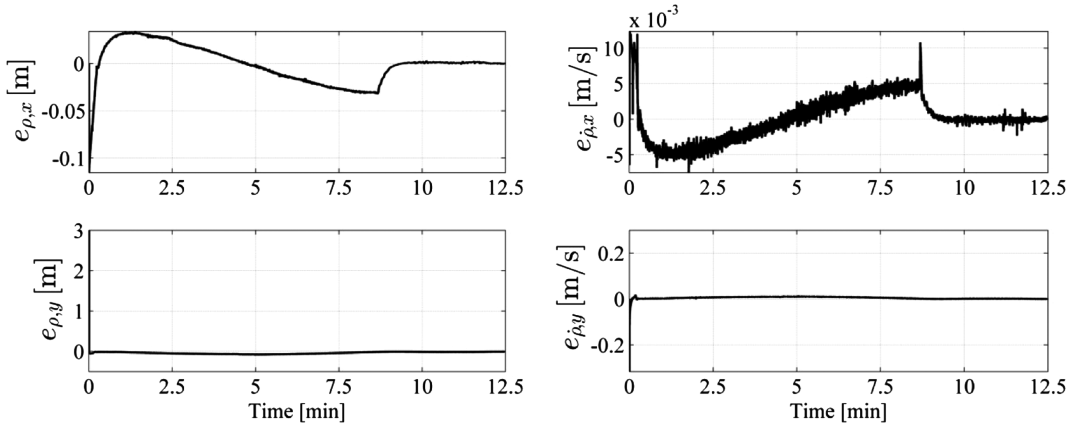

a) b)

Fig. 7 Relative errors for R&D maneuver: a) position; b) velocity.

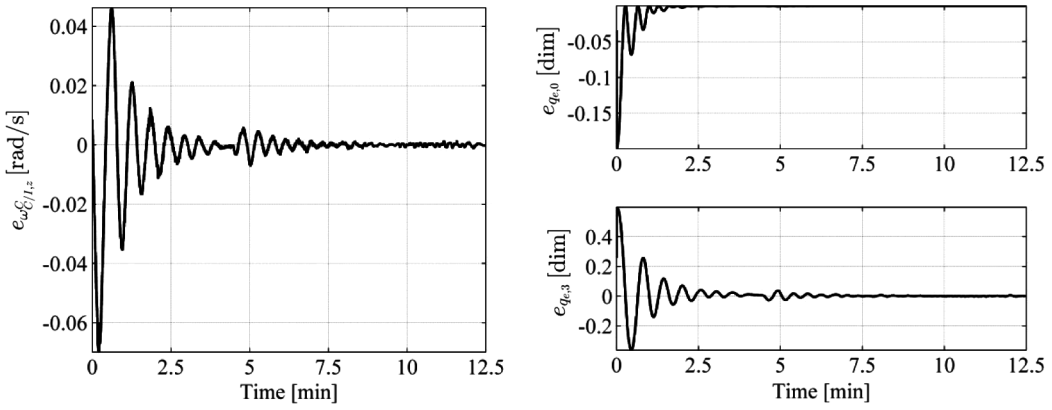

a) b)

Fig. 8 Errors for R&D maneuver: a) absolute angular velocity; b) relative quaternion.

vehicle body-fixed reference frame, respectively, which are required to emulate the orbital motion; the right side of the same figure shows the terms $\check{\boldsymbol{f}}_{\text{control},C}$ and $\check{\boldsymbol{T}}_{\text{control}}$ reported in Eq. (59) due to the SDRE controller.

Finally, Table 2 reports the accuracy values corresponding to NM- and DA-based algorithms. The obtained results show that the DA-based algorithm gives the same order of magnitude of accuracy as the NM algorithm.

Table 2 Accuracy of NM and DA SDRE algorithms for close range R&D maneuver

	Accuracy, $t = t_f$			
Algorithm	$\|\check{\boldsymbol{e}}_\rho\|$, m	$\|\check{\boldsymbol{e}}_{\dot\rho}\|$, m/s	$\|\check{\boldsymbol{e}}_{\omega^C_{C,I}}\|$, rad/s	$\|\check{\boldsymbol{e}}_{\boldsymbol{q}}\|$, dim
DA based	$8.8e-03$	$1.12e-03$	$2.1e-04$	$4.5e-03$
NM	$8.03e-03$	$1.0e-03$	$3.6e-04$	$4.3e-03$

B. Final Approach to Dock a Tumbling Target

The length, time, and mass scale factors exploited to scale the control and the inertial and the gravitational forces/torques for the TEAMS platform are, respectively, $l = 0.2769$, $t = 0.625$, and $k = 0.046$ for this scenario. These values are also exploited to scale the tumbling motion of the target spacecraft, which is numerically simulated by the onboard computer of the TEAMS vehicle by integrating Eqs. (62–64). It is worth mentioning that the maximum time to simulate the maneuver is 10 min.

Let us note that, during the final approach, the chaser satellite has to track a specific velocity profile along the $-\hat{\boldsymbol{j}}_T$ versor to approach the target. In Fig. 10, the scaled reference trajectory is depicted; here, the final position of the virtual target vehicle is illustrated, assuming that at the beginning of the maneuver its body reference frame coincides with the versors of the HT coordinate system (gray arrows). Note that here the HT represents the R reference frame introduced in Sec. VIII.

The SDRE/DA controller design is based on a scaled version of the unperturbed dynamic model (52), where $\boldsymbol{\rho}^H$ and $\boldsymbol{\omega}^H_{H,I}$ are replaced by $\boldsymbol{\rho}^R = \boldsymbol{r}^R_C - \boldsymbol{r}^R_R$ and $\boldsymbol{\omega}^R_{R,I}$, respectively. The weighting matrices Q and Z are positive definitive and constant and they are set to

$$
\begin{aligned}
Q &= \text{diag}([\,Q_{11} \quad Q_{22} \quad 0 \quad Q_{33} \quad Q_{44}\,]) \\
Z &= \text{diag}([\,Z_{11} \quad Z_{22}\,]) \\
Q_{11} &= \text{diag}([\,5e-2 \quad 5e-2 \quad 1e-6\,])\ (1/\text{m})^2 \\
Q_{22} &= \text{diag}([\,5 \quad 5 \quad 10e-4\,])\ (\text{s/m})^2 \\
Q_{33} &= \text{diag}([\,1e-7 \quad 1e-7 \quad 10e-4\,])\ \text{s}^2 \\
Q_{44} &= [I]_{4\times4}1e-4\ (\text{s}^2/\text{m})^2 \\
Z_{11} &= \text{diag}([\,5 \quad 5 \quad 1.5e-3\,])\ (\text{s}^2/\text{m})^2 \\
Z_{22} &= \text{diag}([\,1e-4 \quad 1e-4 \quad 1e-8\,])\ (\text{s}^2/\text{kgm}^2)^2 \qquad (71)
\end{aligned}
$$

Note that the preceding matrices are referred to the orbital controller; this means that they have to be scaled according with length, time, and mass scale factors.

Figures 11 and 12 show the position and velocity error components as well as the angular rate and relative quaternion error, as defined by Eq. (70). At the end of the maneuver, the relative position error is about $3.36e-3$ m, whereas the relative velocity error is about $1.743-4$ m/s. The large-amplitude oscillations seen in the angular rate and quaternion error plot are due to the big attitude error at the beginning of the maneuver; in fact, because the SDRE is designed to track a reference signal, the control signal depends on the difference between the actual state and the reference state, which is significant at the initial time step because of the initial orientation of the TEAMS vehicle. Moreover, the system response is due to the choice of weighting matrices in Eq. (71); they are set mainly to allow the docking within the simulation time.

Figure 13 illustrates both the scaled gravitational and inertial force/torque (left side of the figure) and the controller force/torque (right side of the figure), where forces are expressed in the table reference frame and torques are expressed in the vehicle body-fixed coordinate system.

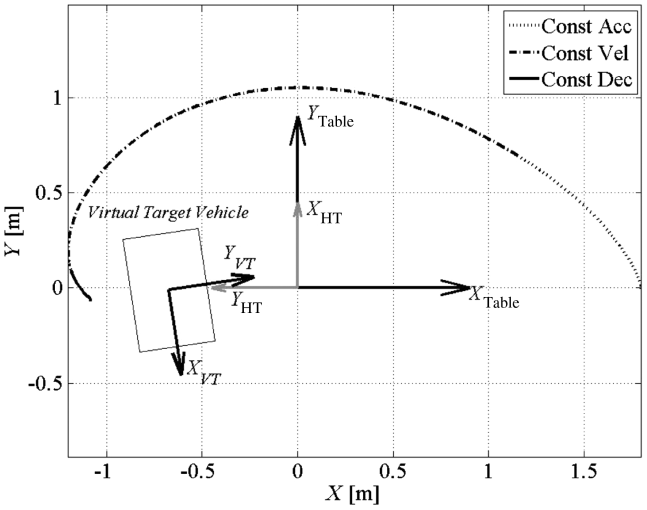

Fig. 10 Reference trajectory on frictionless surface [constant acceleration (Const Acc); constant approaching velocity (Const Vel); constant deceleration (Const Dec)].

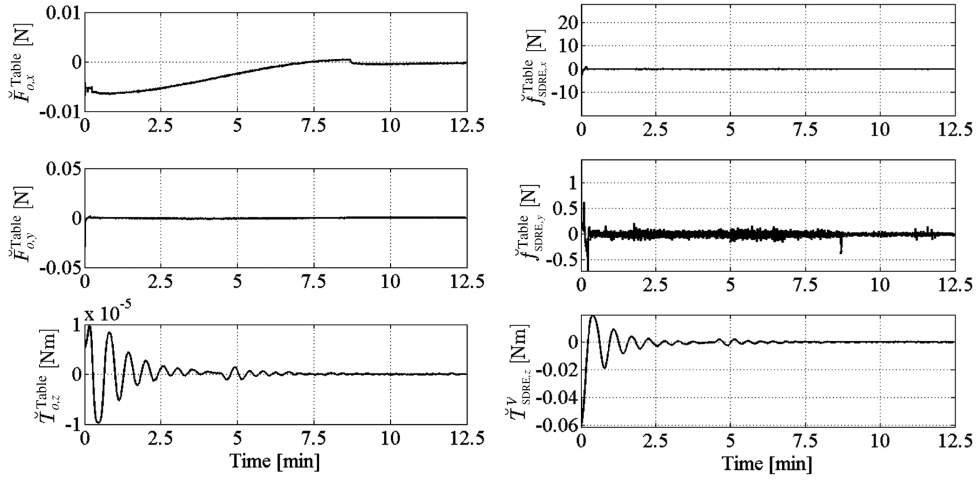

a) b)

Fig. 9 Scaled force/torque for R&D maneuver: a) gravitational and inertial; b) controller.

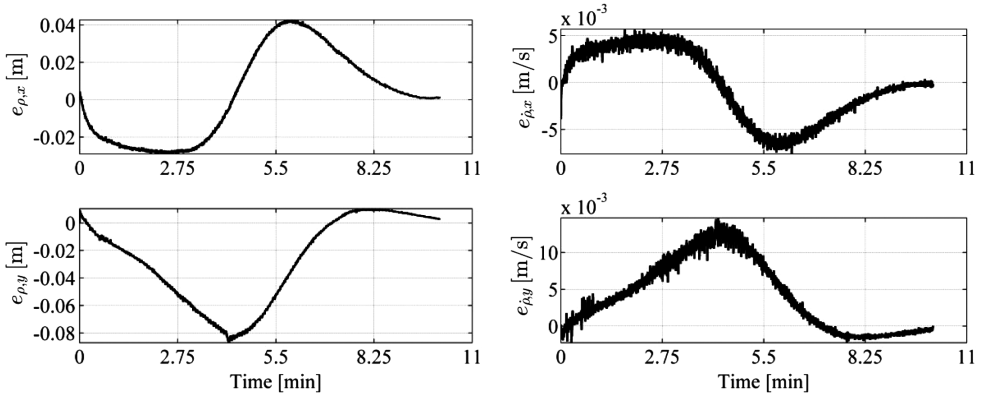

a) b)

Fig. 11 Relative error for final approach maneuver: a) position; b) velocity.

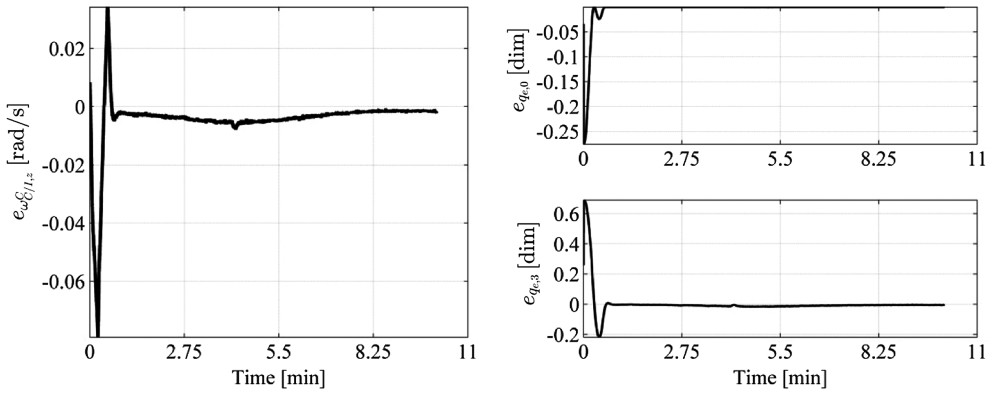

a) b)

Fig. 12 Errors for final approach maneuver: a) angular rate error; b) relative attitude error.

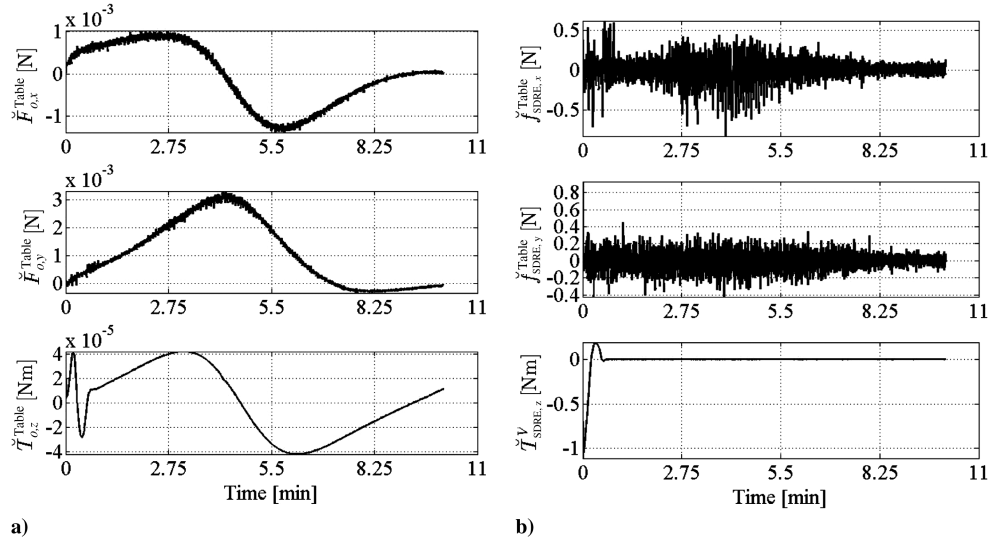

a) b)

Fig. 13 Scaled force/torque final approach maneuver: a) gravitational and inertial; b) controller.

Finally, Table 3 reports the accuracy values corresponding to NM- and DA-based algorithms for the SDRE solution related to the simulated maneuvers. It is worth observing that the DA-based algorithm for the SDRE solution gives the same order of magnitude of accuracy with respect to the "classical" Newton approach.

C. Computational Cost Analysis

In this subsection, the time required by the nonlinear SDRE controller to run on the TEAMS onboard computer is discussed. Table 4 shows the controller execution time for NM- and DA-based methods when a close-range R&D maneuver is simulated. Let us point out that these values are referred to a single experiment and therefore they provide an indication of computational performance of the investigated methods.

As shown in Table 4, the execution time corresponding to each SDRE algorithm is lower than the sampling time, that is, 0.1 s (10 Hz). However, different from results illustrated by the authors of this paper in [36,37], the computational benefit of the DA-based algorithm with respect to the Newton approach is not surprising anymore: In fact, the use of the DA-based algorithm allows reducing

Table 3 Accuracy due to SDRE algorithms for final approach simulated maneuver

	Accuracy, $t = t_f$			
Algorithm	$\|\check{\boldsymbol{e}}_\rho\|$, m	$\|\check{\boldsymbol{e}}_{\dot{\rho}}\|$, m/s	$\|\check{\boldsymbol{e}}_{\boldsymbol{\omega}_{\mathcal{C}_t}^{\mathcal{C}}}\|$, rad/s	$\|\check{\boldsymbol{e}}_{\boldsymbol{q}_e}\|$, dim
DA based	$3.36e-03$	$5.7e-04$	$1.7e-03$	$6.5e-03$
NM	$4.0e-03$	$6.0e-04$	$1.30e-03$	$4.8e-03$

Table 4 Execution time for SDRE algorithms

Algorithm	Execution time, s
DA ($l = 4$; $v = 3$)	0.07
NM (maximum iteration no. $= 5$)	0.084

the execution time to barely 0.014 s. This lack of computational efficiency is probably due to the not optimized implementation of the DA-based algorithm before generating the C code that runs on the onboard computer. This fact causes worsening of the computing performance of the DA-based algorithm. For this reason, our future research will be focused primarily on the improvement of the polynomial evaluation function implemented in MATLAB/Simulink to increase the computational gap between the proposed DA-based algorithm and the classical Newton one.

X. Conclusions

Our work aimed at designing an SDRE controller for an R&D maneuvering problem and testing it on the TEAMS experimental platform developed by DLR Institute of Space Systems to emulate the proximity operations between satellites on the ground. More specifically, DA has been exploited to compute a high-order Taylor expansion of the SDRE solution to reduce the computational effort associated with the ARE solution at each sample time. In fact, the proposed DA-based algorithm does not require any algebraic manipulation to obtain the SDRE solution but only the evaluation of a few polynomial expressions computed offline.

The experimental results have proved the feasibility of computing the solution of the SDRE online on the TEAMS hardware (up to 10 Hz) and also for the studied high-order system (14 variables); nevertheless, the comparison analysis concerning the computing demand of the NM- and DA-based algorithms on the TEAMS computer has not confirmed the good computational performance of the DA-based algorithm given by numerical simulation. This inconsistent result is due to the optimization issue: The function for the evaluation of Taylor polynomial expressions obtained by the COSY-Infinity tool is implemented by MATLAB to generate the corresponding C code by the Real-Time Workshop tool; anyhow, it is not optimized to be handled by the C compiler, affecting the computational performance of the algorithm.

Acknowledgments

This research was supported by the Navigation and Control Systems department of DLR, German Aerospace Center, Institute of Space Systems in Bremen.

References

[1] Fehse, W., *Automated Rendezvous and Docking of Spacecraft*, Cambridge Univ. Press, Cambridge, England, U.K., 2003, pp. 1–29, 180–184, Chaps. 1, 6.

[2] Gonnaud, J. L., Sommer, J., and Tsang, M., "ARPK Design and GNC Performance Evaluation for ATV-Rendezvous," *Proceedings of the 3rd ESA International Conference on Spacecraft Guidance, Navigation and Control Systems*, No. 3, ESA, Noordwijk, The Netherlands, 1997, pp. 95–101.

[3] Subbarao, K., and Welsh, S., "Nonlinear Control of Motion Synchronization for Satellite Proximity Operations," *Journal of Guidance, Control, and Dynamics*, Vol. 31, No. 5, 2008, pp. 1284–1294. doi:10.2514/1.34248

[4] Terui, F., "Position and Attitude Control of a Spacecraft by Sliding Mode Control," *American Control Conference*, Vol. 1, IEEE Publ., Piscataway, NJ, 1998, pp. 217–221. doi:10.1109/ACC.1998.694662

[5] Singla, P., Subbarao, K., and Junkins, J. L., "Adaptive Output Feedback Control for Spacecraft Rendezvous and Docking Under Measurement Uncertainty," *Journal of Guidance, Control, and Dynamics*, Vol. 29, No. 4, 2006, pp. 892–902. doi:10.2514/1.17498

[6] Cloutier, J. R., "State-Dependent Riccati Equation Technique: An Overview," *American Control Conference*, Vol. 2, IEEE Publ., Piscataway, NJ, 1997, pp. 932–936. doi:10.1109/ACC.1997.609663

[7] Hammett, K. D., "Control of Nonlinear Systems via State Feedback State-Dependent Riccati Equation Techniques," Ph.D. Dissertation, U.S. Air Force Inst. of Technology, Wright–Patterson AFB, OH, 1997.

[8] Beeler, S. C., "State-Dependent Riccati Equation Regulation of Systems with State and Control Nonlinearities," NASA TM-2004-213215, 2004.

[9] Cimen, T., "State-Dependent Riccati Equation (SDRE) Control: A Survey," *17th World Congress, the International Federation of Automatic Control*, Vol. 17, No. 1, International Federation of Automatic Control, Laxenburg, Austria, 2008, pp. 3761–3775.

[10] Di Mauro, G., Di Lizia, P., and Lavagna, M., "Control of Relative Motion via State Dependent Riccati Equation," *AAS/IAA Astrodynamics Specialist Conference*, Vol. 142, Univelt, San Diego, CA, 2012, pp. 909–928.

[11] Erdem, E. B., and Alleyne, A. G., "Experimental Real-Time SDRE Control of an Underactuated Robot," *40th IEEE Conference on Decision and Control*, Vol. 3, IEEE Publ., Piscataway, NJ, 2001, pp. 2986–2991. doi:10.1109/.2001.980731

[12] Dang, P., and Lewis, F. L., "Controller for Swing-Up and Balance of Single Inverted Pendulum Using SDRE-Based Solution," *31st Annual Conference of IEEE Industrial Electronics Society*, IEEE Publ., Piscataway, NJ, 2005, pp. 304–309. doi:10.1109/IECON.2005.1568921

[13] Menon, P. K., Lam, T., Crawford, L. S., and Cheng, V. H., "Real-Time Computational Methods for SDRE Nonlinear Control Missiles," *American Control Conference*, Vol. 1, IEEE Publ., Piscataway, NJ, 2002, pp. 232–237. doi:10.1109/ACC.2002.1024809

[14] Cimen, T., "Systematic and Effective Design of Nonlinear Feedback Controllers via the State-Dependent Riccati Equation (SDRE) Method," *Annual Review in Control*, Vol. 34, No. 1, 2012, pp. 32–51. doi:10.1016/j.arcontrol.2010.03.001

[15] Massari, M., and Zamaro, M., "Application of SDRE Technique to Orbital and Attitude Control of Spacecraft Formation Flying," *Acta Astronautica*, Vol. 94, No. 1, 2013, pp. 409–420. doi:10.1016/j.actaastro.2013.02.001

[16] Hammett, K. D., Hall, C. D., and Ridgely, D. B., "Controllability Issues in Nonlinear State-Dependent Riccati Equation Control," *Journal of Guidance, Control, and Dynamics*, Vol. 21, No. 5, 1998, pp. 767–773. doi:10.2514/2.4304

[17] Bini, D. A., Iannazzo, B., and Meini, B., "Numerical Solution of Algebraic Riccati Equations," Soc. for Industrial and Applied Mathematics, Philadelphia, 2012, pp. 83–120, Chap. 3.

[18] Kleinman, D. L., "On an Iterative Technique for Riccati Equations Computations," *IEEE Transactions on Automatic Control*, Vol. 13, No. 1, 1968, pp. 114–115. doi:10.1109/TAC.1968.1098829

[19] Imae, J., Sagami, H., Kobayashi, T., and Zhai, G., "Nonlinear Control Design Method Based on State-Dependent Riccati Equation (SDRE) via Quasi-Newton Method," *43rd IEEE Conference on Decision and Control*, Vol. 3, IEEE Publ., Piscataway, NJ, 2004, pp. 2740–2741. doi:10.1109/CDC.2004.1428876

[20] Cherfi, L., Abou-Kandil, H., and Bouries, H., "Iterative Method for General Algebraic Riccati Equation," *Proceedings of International Conference on Automatic Control and System Engineering*, Cairo International Conference Center, Cairo, 2005.

[21] Ritt, J., *Differential Equations from the Algebraic Standpoint*, Vol. 1, American Mathematical Soc. Colloquium Publ., Providence, RI, 1932, pp. 1–31.

[22] Berz, M., *Modern Map Methods in Particle Beam Physics*, Academic Press, New York, 1999, pp. 81–117, Chap. 2.

[23] Di Lizia, P., Armellin, R., and Lavagna, M., "Application of High Order Expansions of Two-Point Boundary Value Problems to Astrodynamics," *Celestial Mechanics and Dynamical Astronomy*, Vol. 102, No. 4, 2008, pp. 355–375. doi:10.1007/s10569-008-9170-5

[24] Xin, M., and Balakrishnan, S. N., "A New Method for Suboptimal Control of a Class of Non-Linear Systems," *Optimal Control Applications and Methods*, Vol. 26, No. 2, March 2004, pp. 55–83. doi:10.1002/(ISSN)1099-1514

[25] Bartels, R. H., and Stewart, G. W., "Solution of the Matrix Equation $AX + XB = C$," *Communications of the ACM*, Vol. 15, No. 9, 1972, pp. 820–826. doi:10.1145/361573.361582

[26] Alfried, K., Vadali, S. R., Gurfil, P., How, J., and Breger, L., "Spacecraft Formation Flying: Dynamic, Control and Navigation," Elsevier, New York, 2010, pp. 59–82, Chap. 4.

[27] Kechichian, J. A., "Motion in General Elliptic Orbit with Respect to a Dragging and Precessing Coordinate Frame," *Journal of Astronautical Sciences*, Vol. 46, No. 1, 1998, pp. 25–46.

[28] Theron, A., Karai-Zaitri, M., Arzelier, D., and Louembert, C., "Nonlinear and Linear Local Cartesian Relative Motion State Models for J2 Perturbed Elliptical Orbits," *21st International Symposium on Space Flight Dynamics*, Université de Toulouse, Toulose, France, 2009.

[29] Chen, W., and Jing, W., "Differential Equations of Relative Motion Under the Influence of J2 Perturbation and Air Drag," *AIAA Space 2010 Conference & Exposition*, AIAA, Reston, VA, 2010. doi:10.2514/6.2010-8758

[30] Wertz, J. R., *Spacecraft Attitude Determination and Control*, Kluwer Academic, Norwell, MA, 1978, pp. 487–558, Chaps. 15–16.

[31] Cloutier, J. R., and Stansbery, D. T., "Capability and Art of State-Dependent Riccati Equation-Based Design," *American Control Conference*, Vol. 1, IEEE Publ., Piscataway, NJ, 2002, pp. 86–91. doi:10.1109/ACC.2002.1024785

[32] Lee, D., and Pernicka, H., "Integrated System for Autonomous Proximity Operation," *International Journal of Aeronautical and Space Sciences*, Vol. 12, No. 1, 2011, pp. 43–56. doi:10.5139/IJASS.2011.12.1.43

[33] Lee, D., and Pernicka, H., "Optimal Control for Proximity Operations and Docking," *International Journal of Aeronautical and Space Sciences*, Vol. 11, No. 3, 2006, pp. 206–220. doi:10.5139/IJASS.2010.11.3.206

[34] Clohessy, W. H., and Wiltshire, R. S., "Terminal Guidance System for Satellite Rendezvous," *Journal of Aerospace Science*, Vol. 27, No. 9, 1960, pp. 653–658. doi:10.2514/8.8704

[35] Schlotterer, M., and Theil, S., "Testbed for On-orbit Servicing and Formation Dynamics Emulation," *AIAA Guidance, Navigation, and Control Conference*, AIAA, Reston, VA, 2010. doi:10.2514/6.2010-8108

[36] Di Mauro, G., Di Lizia, P., Armellin, R., and Lavagna, M., "Novel Nonlinear Control Approach for Rendezvous and Docking Maneuvering," *63rd International Astronautical Congress*, Curran Associates, Red Hook, NY, 2012, pp. 5357–5365.

[37] Di Mauro, G., Di Lizia, P., Armellin, R., and Lavagna, M., "Nonlinear Control of Leader-Follower Formation Flying," *1st IAA Conference on Dynamics and Control of Space Systems*, Vol. 145, Univelt, San Diego, CA, 2012, pp. 215–230.